UNIVERSIDAD DE GRANADA

Facultad de Ciencias

GRADO EN FÍSICA

TRABAJO FIN DE GRADO

Measurement of magnetic moment of an electronic product using fluxgates 3D

Presentado por:
D. Víctor Vegas Luque

Curso Académico 2021/2022

Resumen

En este trabajo se usará el método computacional de PSO para aproximar los campos magneticos de diferentes dispositivos electrónicos. Se indagará en el procedimiento de medida de campos magneticos dentro de una celda de bobinas mangeticas (MCF), y el trabajo previo a la medida. Finalmente, se discutirán como de precisas son estas aproximaciones y en que rango son válidas.

Abstract

In this thesis we will use the PSO computational method to approximate the magnetic field of different electronic elements from a satellite. We will inquire in the procedure used for measuring magnetic fields inside a Magnetic Coil Facility (MCF), and the work that has to be done prior to the measurements. Finally, we will discuss how precise this approximations are and where they are valid.

Agradecimientos

A pesar de que esta este trabajo este en inglés las personas a las que me gustaría agradecer entienden todas perfectamente el español y no todas entienden el inglés, así que la escribiré en español.

Primeramente, me gustaría agradecer a mi tutor del TFG Andrés Roldán Aranda, por no solo guiarme durante la realización de esta tesis, si no también por introducirme al mundo real, donde los físicos no solo viven de calcular el número de microestados posibles o de resolver ecuaciones de Schrödinger en pozos cuadrados.

También, habría sido impensable realizar esta tesis sin la ayuda de Juan Francisco Gómez Lopera, que a pesar de no haber sido mi tutor, ha prestado su ayuda en todo momento sin recibir nada a cambio.

Tengo que destacar la ayuda que me ha proporcinado mi amigo y vecino de enfrente, José Alberto Gómez García, estudiante de ingeniería informática (y esperemos que ingeniero informático de aquí a un mes) al que torturaba con mis preguntas de Python.

No podía faltar mencionar a mis amigos y amigas de mi colegio mayor y de la facultad, entre los que no paramos de comentar que ojala se acabemos ya la carrera, pero realmente ninguno quiere que se acabe.

Y como último y más importante, a mi familia y en especial a mis padres, no solo por darme la oportunidad de poder estudiar fuera de casa, sino por educarme y hacer que sea la persona que soy.

Contents

1 Introduction **5**

2 Theoretical foundation **6**

2.1 Fundamentals of electromagnetism 6

2.2 Dipole Approximation 7

2.3 Quadrupole Approximation 8

3 Theoretical Validation **10**

3.1 Quadrupole approximation 10

4 Methodology and analysis **15**

4.1 Soft Iron Calibration 15

4.1.1 Magnetometer calibration 15

4.1.2 Process of calibrating 17

4.2 The Magnetic Coil Facility 18

4.2.1 Canceling Earth's magnetic field 19

4.2.2 Deperming process 20

4.2.3 Measuring in the MCF 24

4.3 Optimization algorithm 28

4.3.1 PSO Algorithm 28

4.3.2 Fitness function 29

5 Results and discussion **30**

5.1 The importance of deperming 30

5.2 Comparing Our PSO Data with ESA's 33

5.3 Validity of approximations 36

6 Conclusions **39**

References **40**

1 Introduction

Nowadays, many satellites in outer space come equipped to measure magnetic fields. Since these devices create their own magnetic fields, they must be considered for a faithful measure. As an inspiration for this thesis, we will consider Ulysses satellite, a joint work between NASA and European Space Agency (ESA). This satellite objective was to investigate the magnetic fields of the Sun. Among its findings we can find that the solar winds weaken over time and that the Sun's magnetic field reverses every 11 years. This mission lasted 18 years and (almost) 9 months, four times longer than expected; and it could not have been done without the proper previous work, which we intend to dive into [1].

In this work, we aim to inquire about the research previously done by Yako Irusta Salles [2], and previous to him Pedro Manuel Vizcaíno Delgado [3]. Just like their works, this thesis is meant to be a foundation for future works. This thesis will be highly experimental, but not in the sense that we will be measuring the different of a satellite. Instead we will set a solid basis in which future people can work in.

Most of the experimental work will be done in the laboratories of Grupo de Electrónica Aeroespacial of Universidad de Granada, also known as GranaSAT. We will use fluxgate magnetometers, which will allow us to measure fields of the orders of nT.

Firstly, we will use Maxwell's equations to set our framework, which will be necessary to understand the behaviour of multipolar approximations for the magnetic field. Since dipolar approximations where already heavily discussed in Yako's work [2], we will mainly inquire in the quadrupolar approximations.

One of the main focus of our work will be to fully understand the measuring process. We will tackle problems such as the calibration process for magnetometers or the demagnetization of an electronic device.

To approximate the magnetic field of an electronic device we will use a Particle Swarm Optimization method, also known as PSO. This is a heuristic algorithm that will allow us to optimize a given function to approximate our object of study to a given model. In particular, we will approximate to three different models: 1 dipole, 2 dipoles, and 1 dipole and 1 quadrupole.

Finally, we will work with some data proportioned to us by ESA [4] to find the importance of the demagnetization process and to see how our PSO programs work with real data. We will discuss how good our approximations are and where they are valid. We will also give some indications for future works of parts if this thesis that could be expanded upon.

The reason most of the data we have worked with has been proportioned by ESA is because most of the work done in this thesis is necessary to carry out this measurements, therefore it is left for future works to inquire in this subject.

All of our work has been condensed not only in this thesis, but also in multiple Python programs that can be found in GranaSAT's GitHub repository [5], which overall extension is 5657 lines of code, distributed in four different Jupyter notebooks [6].

Before moving on, in Fig. 1 we can see a Gantt diagram of how we have spent the time given to carry out this thesis.

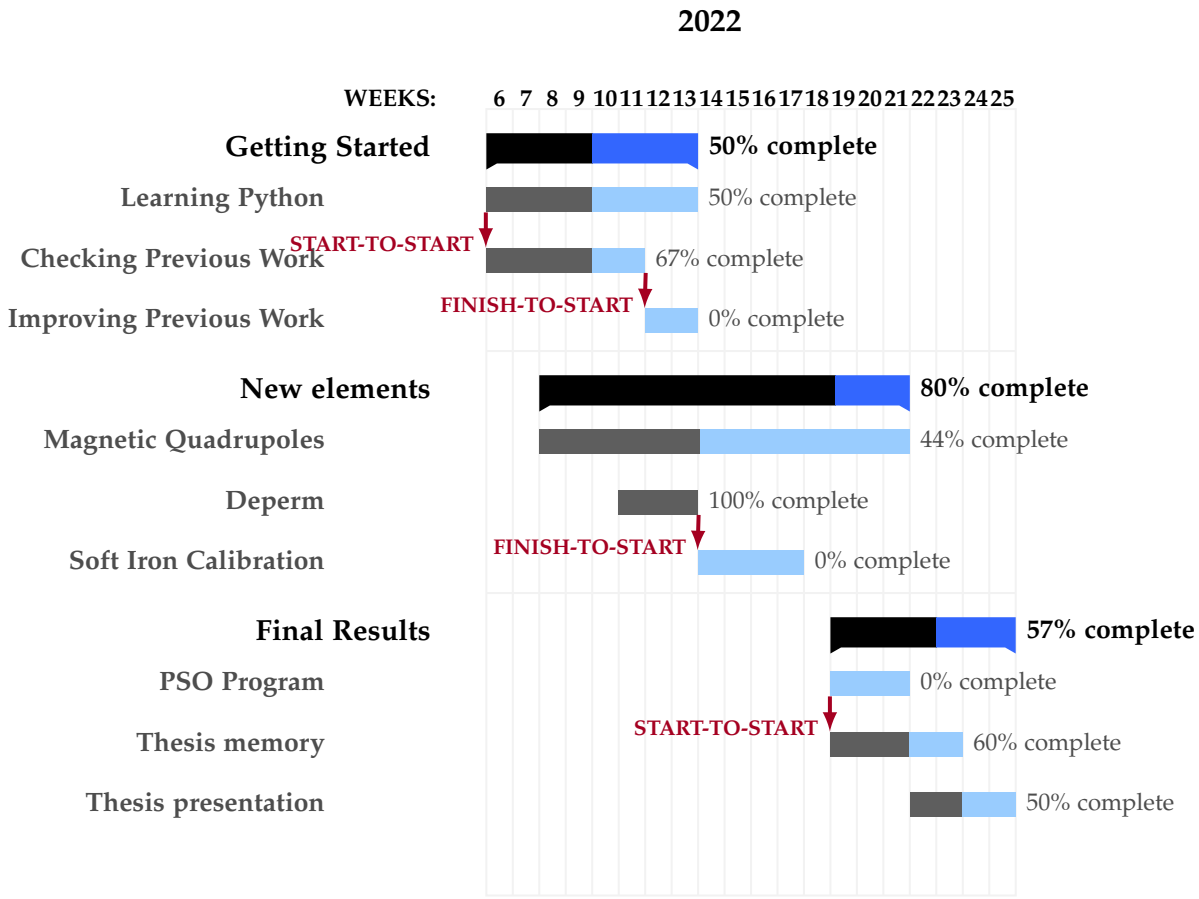

Figure 1: Gantt diagram of the different activities carried out during this thesis.

2 Theoretical foundation

2.1 Fundamentals of electromagnetism

Since we will be working with electromagnetism extensively, it is important that we set a good frame of work. This frame will be described by the famous Maxwell's equations, formulated in 1861 [7]; which are given below:

$$\nabla \cdot \mathbf{E} = \frac{\rho}{\epsilon_0} \tag{2.1}$$

$$\nabla \cdot \mathbf{B} = 0 \tag{2.2}$$

$$\nabla \times \mathbf{E} = \frac{\partial \mathbf{B}}{\partial t} \tag{2.3}$$

$$\nabla \times \mathbf{B} = \mu_0 \left(\mathbf{J} + \epsilon_0 \frac{\partial \mathbf{B}}{\partial t} \right) , \tag{2.4}$$

where $\mathbf{E}$ and $\mathbf{B}$ represent the electric and magnetic field, respectively; ϵ_0 and μ_0 the electric permittivity and magnetic permeability in vacuum, respectively; and $\mathbf{J}$ the density current.

Although Maxwell's equations do describe our framework, they can be tricky to work with. For our work, it will be useful to use the Biot-Savart law, which is given here below:

$$\mathbf{B}(\mathbf{r}) = \frac{\mu_0}{4\pi} \int_C \frac{Id\mathbf{l} \times (\mathbf{r} - \mathbf{r}')}{|\mathbf{r} - \mathbf{r}'|^3} \,, \tag{2.5}$$

where C is the path along the direction of the current I, and ther$\mathbf{r}$ and $\mathbf{r}\prime$ are vectors which represent the distance between the origin and where the field is being calculated and the current element, respectively. A representative figure is shown below:

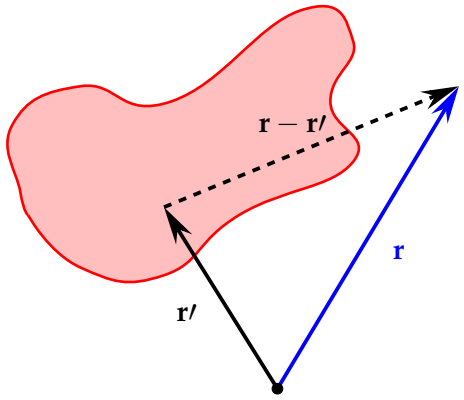

Figure 2: Representative figure of the vectors used in (2.5) .

Looking at Maxwell's second equation (2.2) and remembering the following property of divergence:

$$\nabla \cdot (\nabla \times \mathbf{A}) = 0 \,, \tag{2.6}$$

we introduce the magnetic vector potential $\mathbf{A}$:

$$\mathbf{B} = \nabla \times \mathbf{A} \,, \tag{2.7}$$

which although it may seem tedious to work with, it will be of good use for multipolar expansions, as we will see. Using equations (2.5) and (2.7), we get the expression for the magnetic vector potential:

$$\mathbf{A} = \frac{\mu_0 I}{4\pi} \oint \frac{d\mathbf{r}'}{|\mathbf{r} - \mathbf{r}'|} \,. \tag{2.8}$$

2.2 Dipole Approximation

In this section, we will focus on the calculations of the dipole expressions. We will skip over many steps of the derivation of the expressions, since they can be found in Yako's work [2].

Our starting point will be equation (2.8). We will Taylor expand the integrand as follows:

$$\frac{1}{|\mathbf{r} - \mathbf{r}'|} = \frac{1}{r} + \frac{\mathbf{r} \cdot \mathbf{r}'}{r^3} + \mathcal{O}(\delta^2) \,. \tag{2.9}$$

Plugging in the expression above in (2.8), we get the following:

$$\mathbf{A} = \frac{\mu_0 I}{4\pi}\left(\oint \frac{d\mathbf{r}'}{r} + \oint \frac{\mathbf{r}\cdot\mathbf{r}'}{r^3} d\mathbf{r}' + ...\right) . \tag{2.10}$$

We have to note that for this approximation to hold, we require that the distance of measuring is larger than the region where the current flows.

We can see that the first integral from (2.10) vanishes, since the integral of a closed path is always zero, therefore proving that magnetic monopoles do not exist. The second integral leaves us with a magnetic potential like this:

$$\mathbf{A} = \frac{\mu_0 I}{4\pi r^3} \oint (\mathbf{r}\cdot\mathbf{r}')\, d\mathbf{r}' . \tag{2.11}$$

We define now the magnetic moment as follows:

$$\mathbf{m} = \frac{I}{2}\int \mathbf{r}\times\mathbf{r}' , \tag{2.12}$$

which is a vector that, as shown is Yako's work [2], can be plugged in (2.11), resulting in:

$$A = \frac{\mu_0}{4\pi}\frac{(\mathbf{m}\times\mathbf{r})}{r^3} . \tag{2.13}$$

Using the definition of **B** given in (2.7), and (2.13), we end up with the following expression for the magnetic field of a dipole:

$$\mathbf{B} = \frac{\mu_0}{4\pi}\left(\frac{3(\mathbf{m}\cdot\mathbf{r})\mathbf{r}}{r^5} - \frac{\mathbf{m}}{r^3}\right) . \tag{2.14}$$

A more general expression can be obtained if we treat **r** as the distance from the magnetic dipole to the point we want to measure the magnetic field on:

$$\mathbf{r} = (x-x_0)\hat{\mathbf{x}} + (y-y_0)\hat{\mathbf{y}} + (z-z_0)\hat{\mathbf{z}} , \tag{2.15}$$

which, in combination with (2.14) gives us the expressions for the magnetic field of a dipole centered in (x_0, y_0, z_0):

$$\begin{aligned}
B_x &= \frac{\mu_0}{4\pi}\left(\frac{3\left(m_x(x-x_0)+m_y(y-y_0)+m_z(z-z_0)\right)(x-x_0)}{r^5} - \frac{m_x}{r^3}\right)\\
B_y &= \frac{\mu_0}{4\pi}\left(\frac{3\left(m_x(x-x_0)+m_y(y-y_0)+m_z(z-z_0)\right)(y-y_0)}{r^5} - \frac{m_y}{r^3}\right)\\
B_z &= \frac{\mu_0}{4\pi}\left(\frac{3\left(m_x(x-x_0)+m_y(y-y_0)+m_z(z-z_0)\right)(z-z_0)}{r^5} - \frac{m_z}{r^3}\right) ,
\end{aligned} \tag{2.16}$$

where m_x, m_y and m_z are the value of the magnetic moment in each direction.

2.3 Quadrupole Approximation

In this section we will discuss the quadrupole approximation. Our first instinct would be to apply the same procedure we applied for the dipoles, by continuing the Taylor

expansion from (2.9) and taking higher order terms. However it is not an easy task to find a usable result using this procedure, and it is not well documented. Therefore, we will use an equivalent method.

It is well known that a magnetic quadrupole field can be achieved using Helmholtz Coils set in a particular configuration [8]. This configuration is such that the diameter of the coils should be the same as the distance between them, and the current flows in opposite directions in each coil. For simplicity reasons, we will consider that each coil is made of only a single loop. The geometry of a current loop is shown here below:

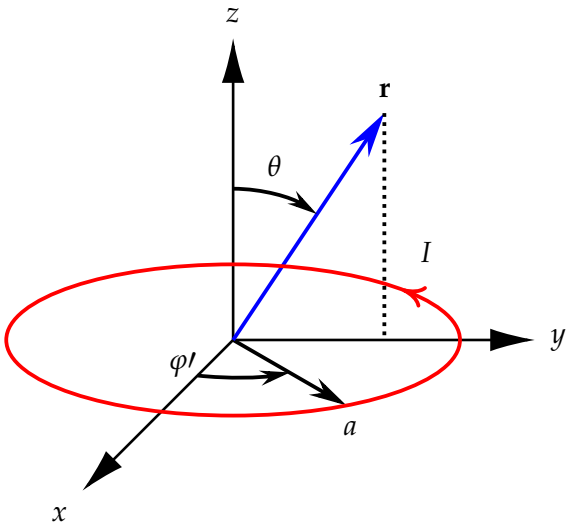

Figure 3: Geometry of a circular current loop.

The general expression for the magnetic vector potential for a closed current loop is the following [9]:

$$A_\varphi(r,\theta) = \frac{\mu_0 I a}{4\pi} \int_0^{2\pi} \frac{\cos\varphi' \, d\varphi'}{\sqrt{a^2 + r^2 - 2ar\sin\theta\cos\varphi'}} \,, \tag{2.17}$$

where a is the radius of the loop and I the intensity of the current flowing through it. The magnetic field in spherical coordinates can then be calculated as follows:

$$B_r = \frac{1}{r\sin\theta}\frac{\partial}{\partial x}\left(\sin\theta A_\varphi\right) \tag{2.18}$$

$$B_\theta = -\frac{1}{r}\frac{\partial}{\partial x}\left(r A_\varphi\right) \tag{2.19}$$

$$B_\varphi = 0 \,. \tag{2.20}$$

Now another problem arises, which is that the expressions for the magnetic field do not have an analytical solution outside of the axis of the loop. The analytical expression for the magnetic field on its axis is as follows [10]:

$$\mathbf{B} = \frac{\mu_0}{4\pi}\frac{2\pi a^2 I}{\left(a^2 + z^2\right)^{3/2}} \,. \tag{2.21}$$

To find the expressions for the magnetic field we will make use of the full elliptic integrals of first and second kind, which are shown below, respectively:

$$K(m) = \int_0^{\frac{\pi}{2}} \frac{d\theta}{\sqrt{1 - m\sin\theta}} \tag{2.22}$$

$$E(m) = \int_0^{\frac{\pi}{2}} \sqrt{1 - m\sin\theta}\, d\theta \ . \tag{2.23}$$

The expression (2.17) can then be expressed as [11]:

$$A_\varphi(r,\theta) = \frac{\mu_0 I a}{4\pi} \frac{4Ia}{\sqrt{a^2 + r^2 + 2ar\sin\theta}} \left[\frac{(2-k^2)K(k^2) - 2E(k^2)}{k^2} \right] \ , \tag{2.24}$$

where the argument of the elliptic integrals k^2 is defined as:

$$k^2 = \frac{4ar\sin\theta}{a^2 + r^2 + 2ar\sin\theta} \ . \tag{2.25}$$

The expressions for the magnetic field components in cartesian coordinates can now be written as:

$$\begin{aligned} B_x &= \frac{Cxz}{2\alpha^2\beta\rho^2} \left[(a^2 + r^2)E(k^2) - \alpha^2 K(k^2) \right] \\ B_y &= \frac{Cyz}{2\alpha^2\beta\rho^2} \left[(a^2 + r^2)E(k^2) - \alpha^2 K(k^2) \right] \\ B_z &= \frac{C}{2\alpha^2\beta} \left[(a^2 - r^2)E(k^2) + \alpha^2 K(k^2) \right] \ , \end{aligned} \tag{2.26}$$

where, to simplify the expressions, we have used the following variables:

$$\begin{gathered} \rho^2 \equiv x^2 + y^2 \ \ ; \ \ r^2 \equiv x^2 + y^2 + z^2 \ \ ; \ \ \alpha^2 \equiv a^2 + r^2 - 2a\rho \\ \beta^2 \equiv a^2 + r^2 + 2a\rho \ \ ; \ \ k^2 \equiv 1 - \alpha^2/\beta^2 \ \ ; \ \ \gamma^2 \equiv x^2 - y^2 \ \ ; \ \ C = \frac{\mu_0 I}{\pi} \ . \end{gathered} \tag{2.27}$$

3 Theoretical Validation

Now that of theoretical framework is set, we will check if the approximations we have presented coincide with measured values. The dipole approximation was discussed in Yako's work [2], and it was proven to be a good approximation for most electronic devices, so we will focus on the quadrupole approximation.

3.1 Quadrupole approximation

We will start discussing the validity of the use of elliptic integrals for our calculations for current loops following expression (2.16). For this we will compare the results with the ones using Biot-Savart. (2.5). To make our graphs easier to interpret, we will work on the XZ-plane and we will assume the Z-axis acts as the loop's axis.

The magnetic field created using both methods is shown below, where we have used a current $I = 1$ A and a radius of $a = 0.3$ cm:

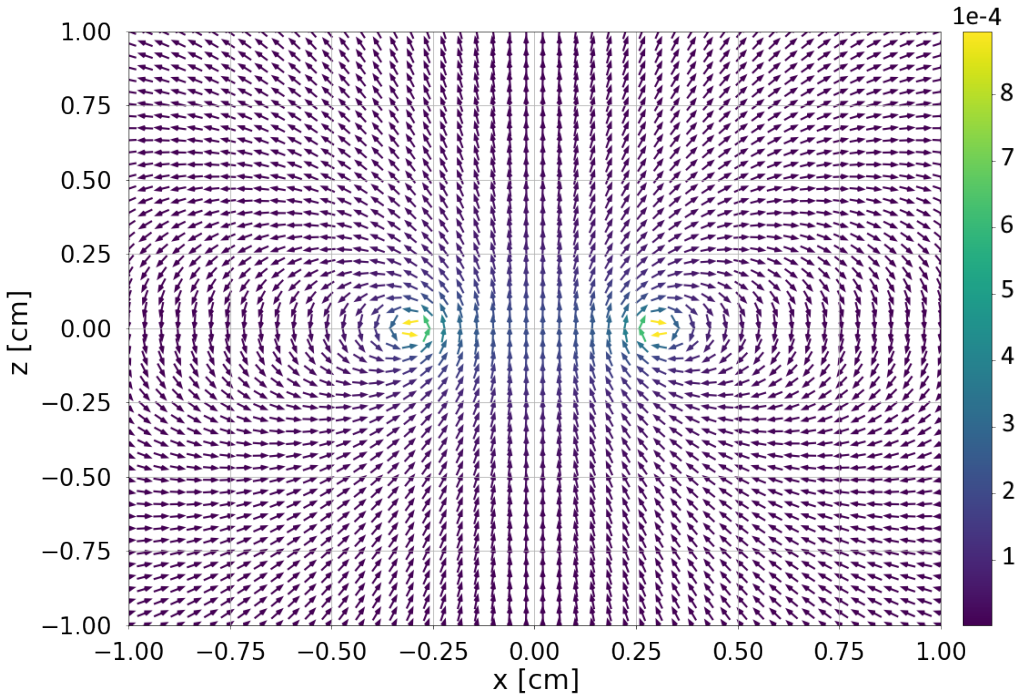

Figure 4: Magnetic field of a current loop on the XZ plane calculated using Biot-Savart (2.5).

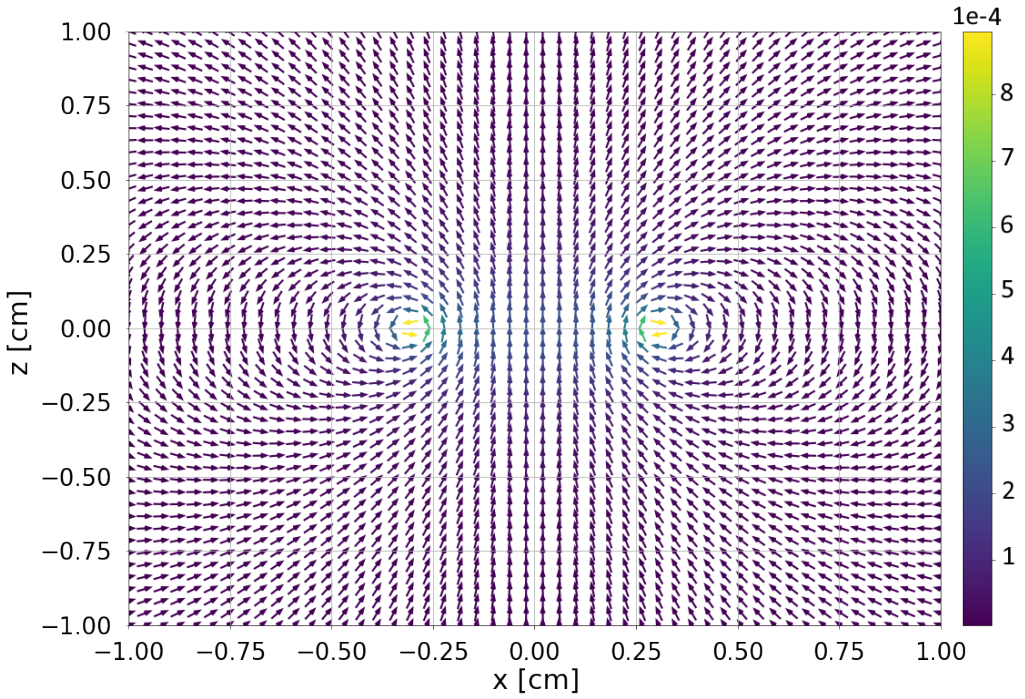

Figure 5: Magnetic field of a current loop on the XZ plane calculated using the expressions (2.26).

As we can see the values for the magnetic field are indistinguishable. We can also check the values for the relative errors:

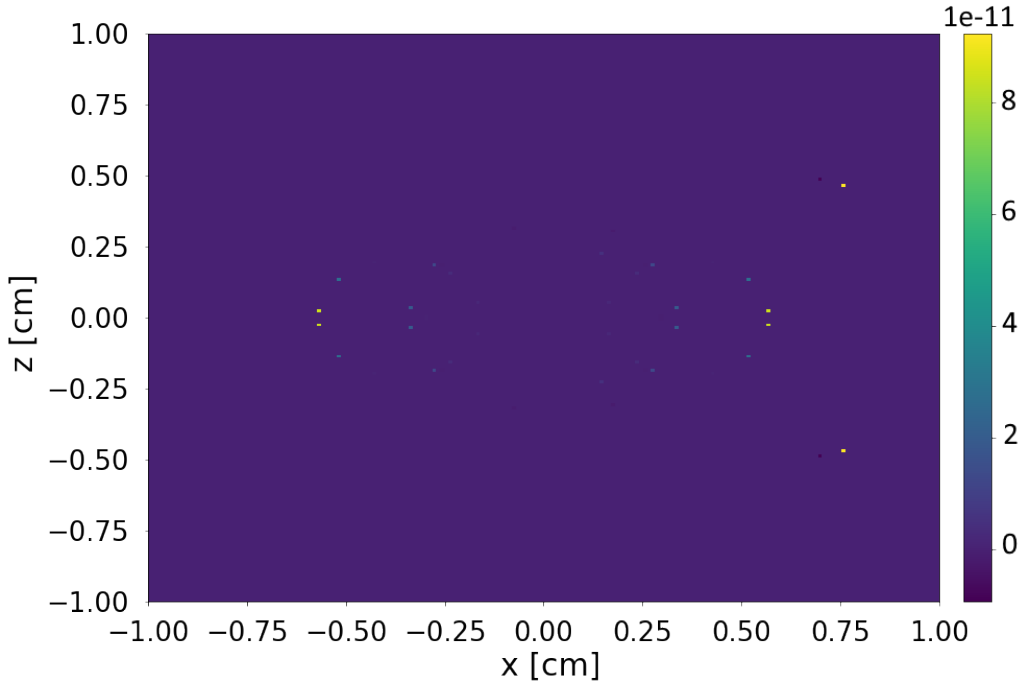

Figure 6: Relative error between Fig. 4 and Fig. 5.

We also see that the difference between bot methods is negligible, therefore proving that the use of elliptic functions is valid. The points in Fig. 6 with higher relative error could be associated to computing error, and since we are working at very small orders of magnitude, even the smaller errors count.

The fact that the results we get are practically identical is not surprising, since the expressions (2.21) can be derived from (2.17) without doing any approximations. The real importance comes from the difference between execution times of both methods, which are shown below

	Biot-Savart	Elliptic Integrals
t_{ex}	23.6 s	1 ms

Table 1: Comparison between running times when calculating the magnetic field of a dipole using Biot-Savart and elliptic integrals.

As we can see, the time difference is quite significant, so we can conclude that using elliptic functions not only helps simplify things up, but also it also make our simulations run faster.

Now that we have a simple way of calculating the magnetic field of a current loop, we can create a quadrupole using two current loops separated by the same distance as their diameter, and having their currents go in opposite directions [8].

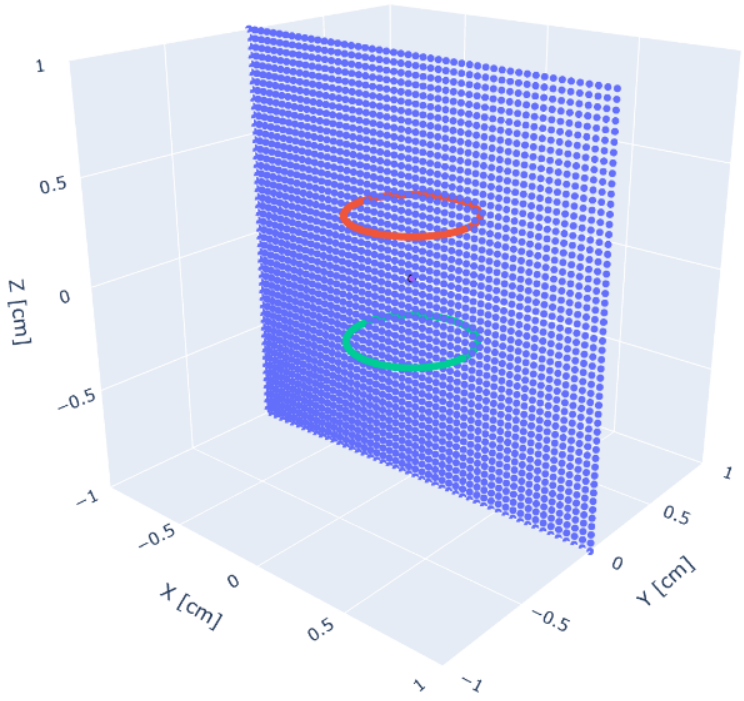

Figure 7: Geometric representation of a magnetic quadrupole created by two current loops.

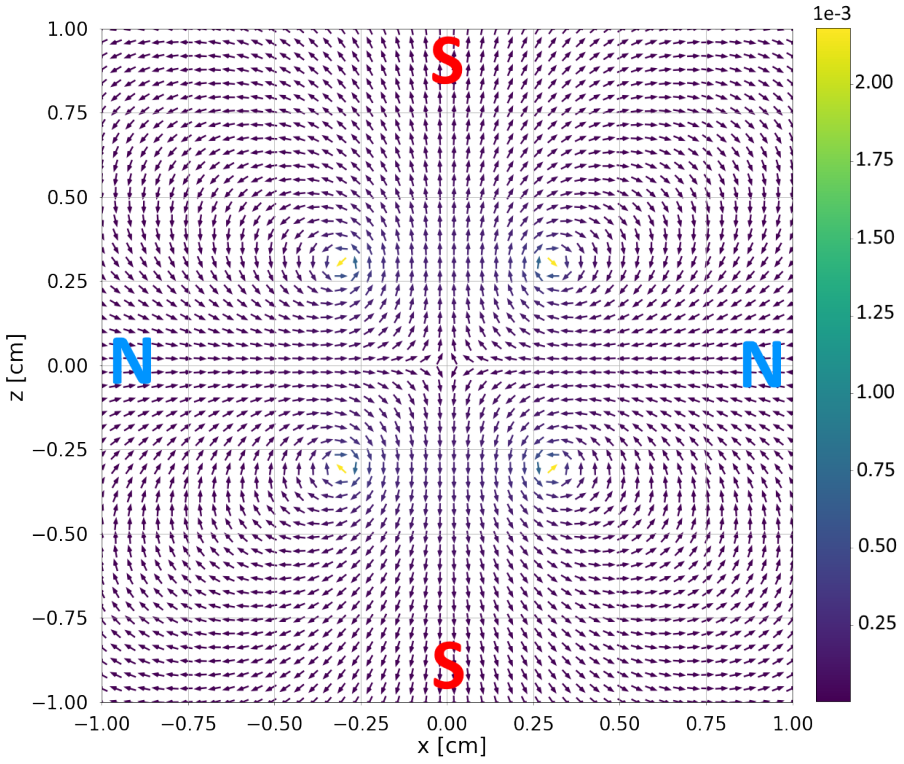

Figure 8: Magnetic field created by a magnetic quadrupole.

The loops coloured in red and green in Fig. 7 represent the current loops with intensity I and $-I$, respectively; and the blue dots represent the points where the field is being measured. In Fig. 8 we can see the four magnetic poles, two North and two South [12].

An arbitrary quadrupole would then be given by 7 components: the radius of the current loops a, the currents I and $-I$ flowing through them, the center point (x_0, y_0, z_0) and an unitary vector that can be expressed as using a polar angle θ (where $\theta = 0$ corresponds with the Z axis) and an azimuthal angle φ:

$$\hat{d} = \sin\theta\cos\varphi\hat{x} + \sin\theta\sin\varphi\hat{y} + \cos\theta\hat{z}\ . \tag{3.1}$$

Here below we can see and example of how an arbitrary quadrupole would look like:

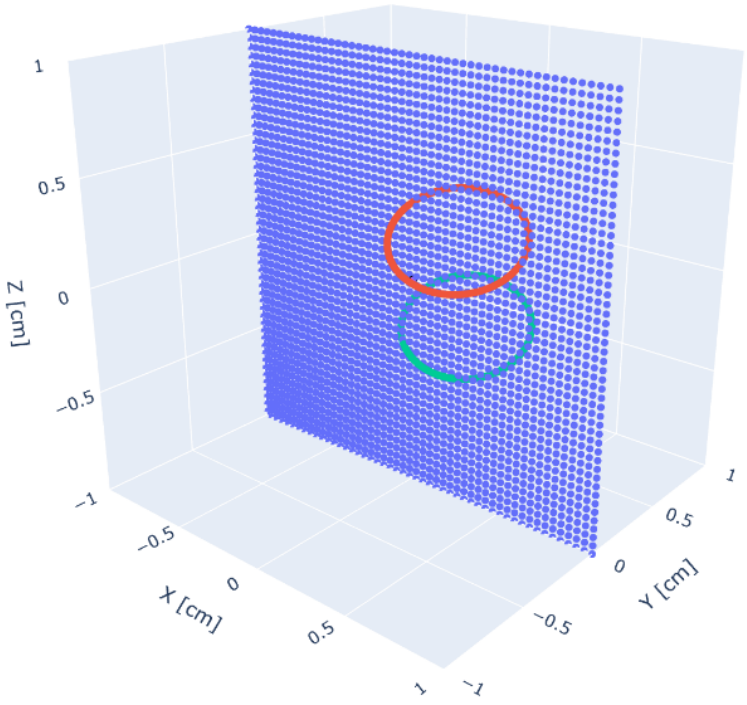

Figure 9: Geometric representation of a magnetic quadrupole created by two current loops which have been rotated and displaced from the origin.

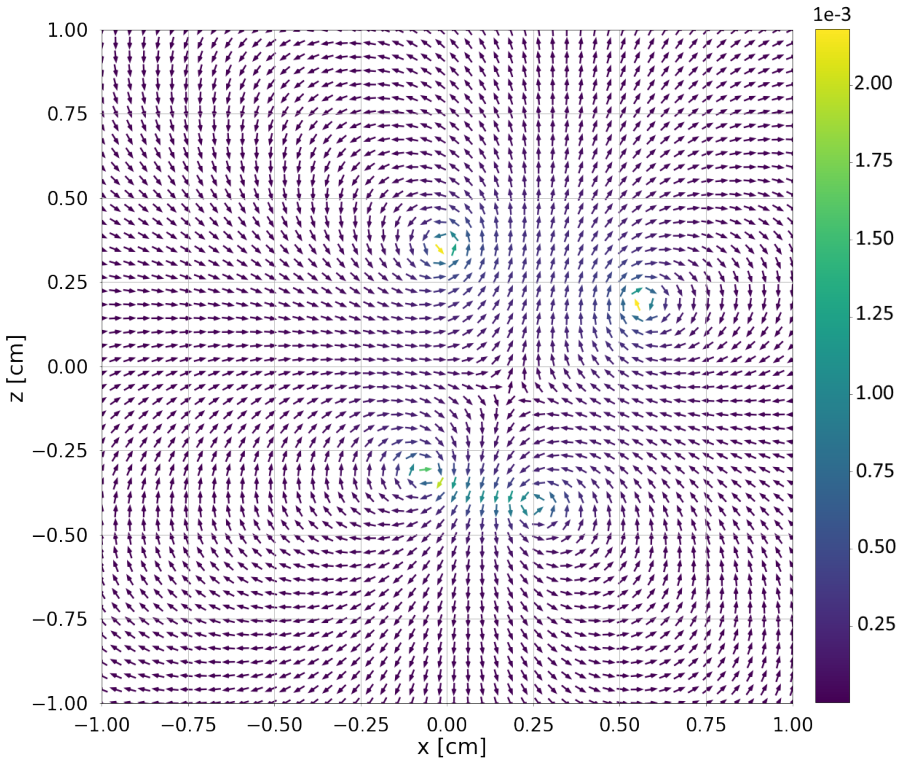

Figure 10: Magnetic field created by an a magnetic quadrupole which has been rotated and displaced from the origin.

In particular, Fig. 9 and Fig. 10 are an example of a quadrupole centered in $(0.2, 0.1, 0)$ for a vector $\hat{d}$ given by $\theta = 30°$ and $\varphi = 30°$, with the same values of a and I used in Fig. 8.

4 Methodology and analysis

4.1 Soft Iron Calibration

Before we do any measurements, it is important that our magnetometers are ready to measure to avoid obtaining unfaithful results. In this section, we will describe the math used for calibrating magnetometers, in a process known as soft iron calibration [13].

4.1.1 Magnetometer calibration

Firstly, we will assume that the magnetic field generated by the earth does not change locally, which is reasonable. Ideally, if we were to rotate our magnetometer describing the surface of a sphere, in the reference system of the magnetometer, the magnetic field would also describe a sphere with radius that of the magnitude of Earth's magnetic field. Such process can be done using a structure that allows us to rotate our magnetometer freely, like the one shown here:

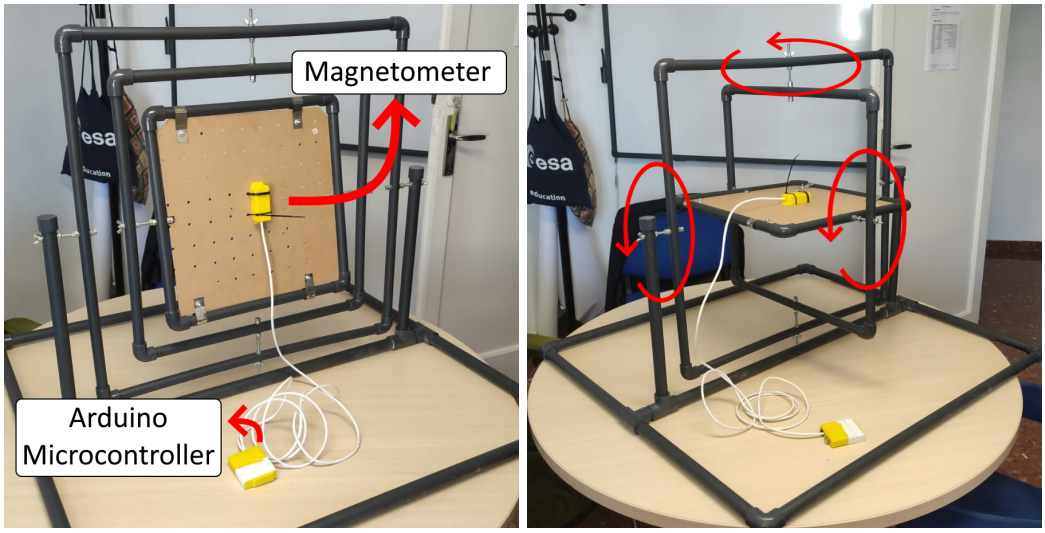

Figure 11: Structure used for calibrating the magnetometer.

The magnetometer is simply strapped into the middle plate, and then the structure is manually spun. In particular the magnetometer used is a LSM9DS0 magnetometer [14], together with and Arduino Pro Mini 328 3.3V/8MHz microcontroller [15].

The raw measures of the magnetic field we expect to get is shown here below:

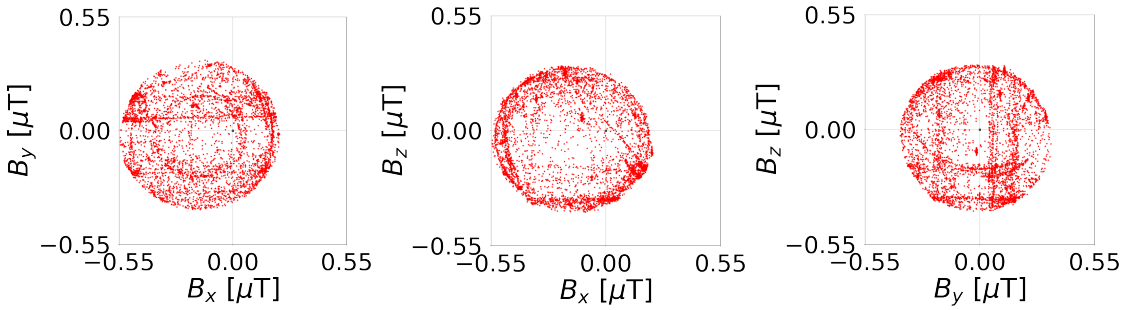

Figure 12: Experimental measures of the magnetic field on each cartesian plane before calibrating.

These experimental results As we can see that the experimental results don't match the ideal scenario, and the measured points appear to describe an ellipsoid instead of a sphere. The main problems resulting to that are:

- The magnetic field is not centered around zero.
- The strength of the magnetic field is measured unevenly between different directions.

The nature of this problems could be of many kinds, like deterioration or internal magnetic fields; but what is important is that it can be accounted for and fixed with the proper software.

4.1.2 Process of calibrating

As we said before, the magnetometer appears to describe an ellipsoid, therefore we aim to reproduce the equation of an ellipsoid. In general, the equation of a conic is given by the following expression [13]:

$$Ax^2 + By^2 + Cz^2 + 2Dxy + 2Exz + 2Fyz + 2Gx + 2Hy + 2Iz + J = 0\ . \tag{4.1}$$

Known the parameters, we can calculate the center of the ellipsoid $\mathbf{P_0}$ this way [13]:

$$\mathbf{Q} = \begin{bmatrix} A & D & E \\ D & B & F \\ E & F & C \end{bmatrix} \ ; \ \mathbf{U} = \begin{bmatrix} G \\ H \\ I \end{bmatrix} \ ; \ \mathbf{P_0} = -\mathbf{Q}^{-1} \cdot \mathbf{U}\ . \tag{4.2}$$

The semi axis of the ellipsoid can then be calculated like [13]:

$$r_i = \left(\frac{\mathbf{P_0}^T \cdot \mathbf{Q} \cdot \mathbf{P_0} - J}{\lambda_i} \right)^{1/2}\ , \tag{4.3}$$

where λ_i (with $i = 1, 2, 3$) are the eigenvalues of $\mathbf{Q}$ with normalized eigenvectors $\mathbf{v_i}$.

The calibration process will then be done in 5 steps [13]:

1. Adjust the experimental measures to an ellipsoid, following equation (4.1).
2. Find the center of the ellipsoid using equations (4.2) and move all experimental measures so the center is at (0,0,0).
3. Align the semi axes with the axes of the reference frame given by $\mathbf{v_i}$. This is done by rotating using the matrix V^{-1}, where V is the 3×3 matrix which has $\mathbf{v_i}$ as its columns.
4. Scale the semi axes so they have the same length, which would be the magnitude of Earth's magnetic field. This process would be achieved using the following matrix

$$R = B_{Earth} \begin{bmatrix} \frac{1}{\lambda_1} & 0 & 0 \\ 0 & \frac{1}{\lambda_2} & 0 \\ 0 & 0 & \frac{1}{\lambda_3} \end{bmatrix}\ . \tag{4.4}$$

5. Rotate back the sphere to the original orientation using V.

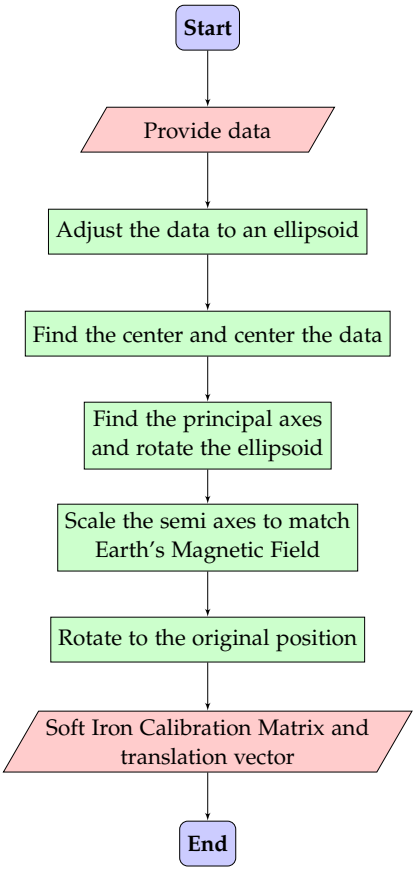

Figure 13: Flow chart of the soft iron calibration process.

The results of the calibration are a translation vector given by P_0 and a matrix which rotates, scales and rotates back (in that order), given by $V \cdot R \cdot V^{-1}$. Once

the calibration is complete, this will allow us transform the data given by our magnetometer to an actual measure of the magnetic field.

In the case of Fig. 12, the final result after applying the soft iron calibration process is:

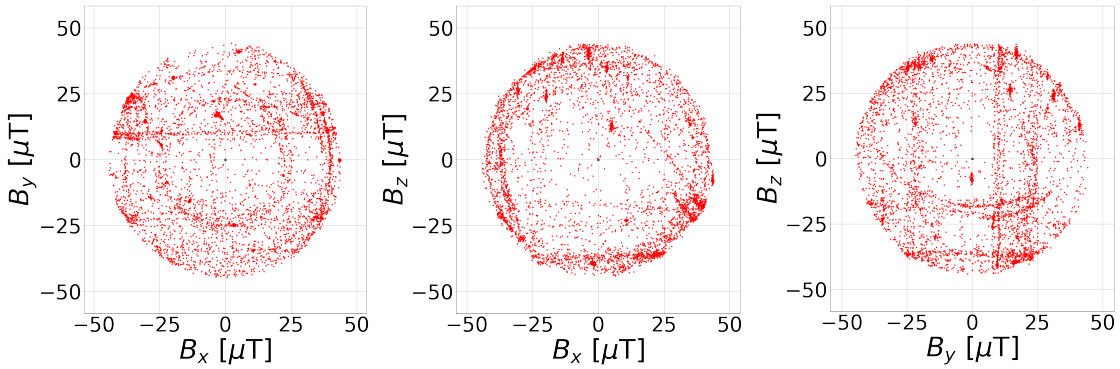

Figure 14: Experimental measures of the magnetic field on each cartesian plane after applying the soft iron calibration process.

Where we have used a value of 43600 ± 160 nT, the value of Earth's magnetic field at Granada, Spain (37° 10′ 13″ N, 3° 36′ 18″ W) on June tenth, two thousand twenty-two [16].

4.2 The Magnetic Coil Facility

In this section we will discuss the process of measuring using the Magnetic Coil Facility (MCF). This facility is a set of Helmholtz coils which aim to cancel Earth's magnetic field inside the facility. The facility is also able to demagnetise an object in a process known as deperming [17]. Here below we can see some pictures of the MCF in the ESA facility:

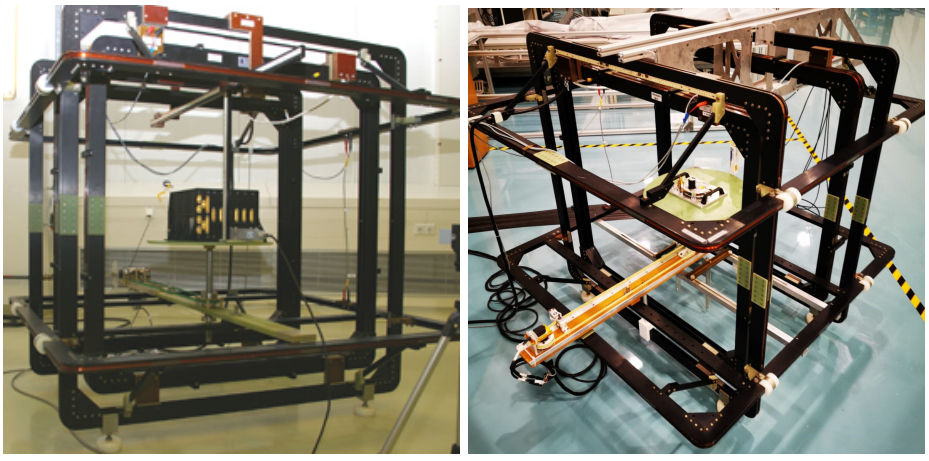

Figure 15: Pictures of the MCF at the ESA Facility [17].

We can also observe the following figure with a 3D model of the MCF, to get a better understanding of the disposition of the coils:

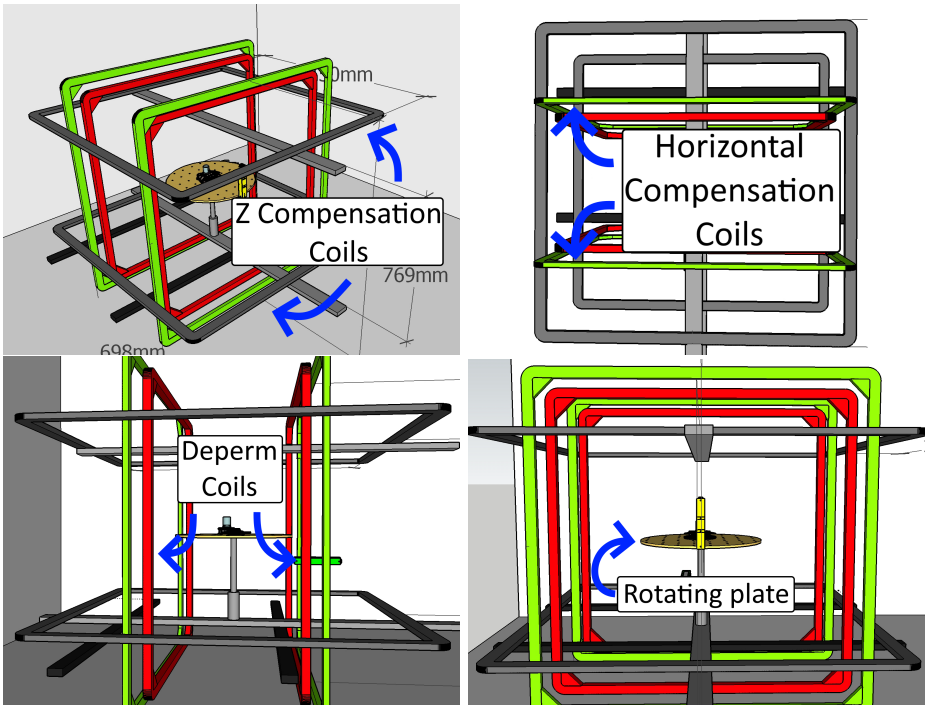

Figure 16: 3D model of the MCF made using Sketchup [2].

The green and grey coils in Fig. 16 are used for canceling Earth's magnetic field, while the red coil is used in the process of deperming.

4.2.1 Canceling Earth's magnetic field

In any reference frame, Earth's magnetic field is given by three components. At first glance we could think that three different coils would be needed, but this is not the case since we could consider that the magnetic field has a vertical and an horizontal component, and align our two coils is such a way that their axes coincide with each component. One could also think that only one coil is needed and, while this is certainly true, it is easier to build a structure with one horizontal and one vertical coil which can be orientated, rather than a single coil that can be freely orientated.

We want to orientate the MCF in such a way that the vertical coils create a field that is opposite to the horizontal one created by Earth. To align the MCF, we will first measure the magnetic field in the reference frame X′, Y′ and Z′ shown in the figure below:

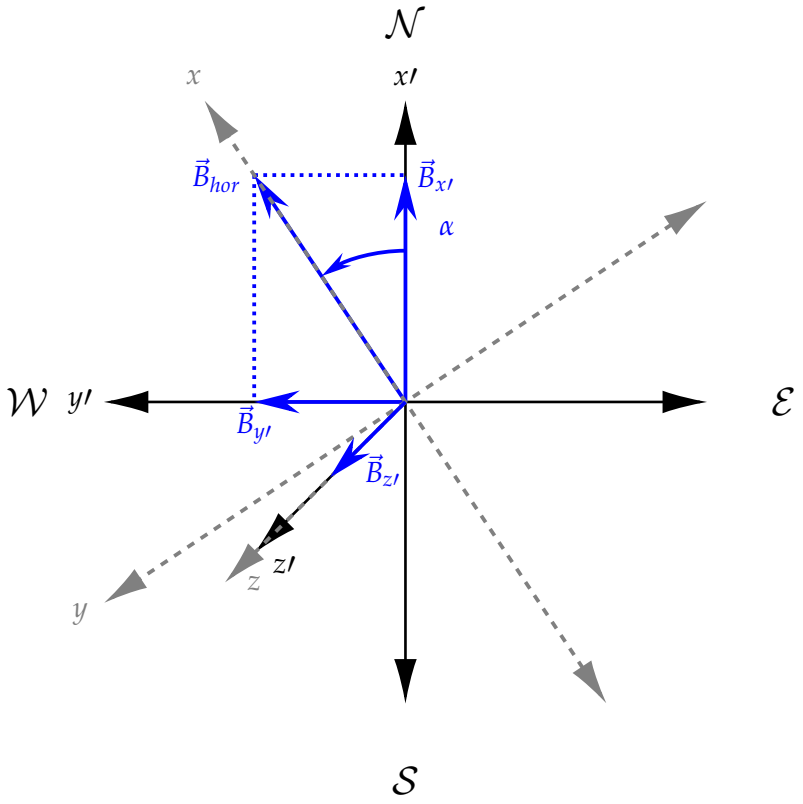

Figure 17: Coordinate system used to align the MCF.

In Fig. 17 $\mathcal{N}$, $\mathcal{S}$, $\mathcal{E}$ and $\mathcal{W}$ represent the four cardinal points. To align the coils with the horizontal component, the MCF should be rotated an angle α, which represents the horizontal orientation with respect to the north and it can be calculated in the following way:

$$\alpha = \arctan \frac{B_{y'}}{B_{x'}} \, . \tag{4.5}$$

Once the MCF is aligned, our reference frame will be given by X, Y and Z from Fig. 17.

4.2.2 Deperming process

The deperming process is a procedure where the magnetic field from an object is erased. The process is done by applying a certain magnetic field varying with time, like the one shown here below [18].

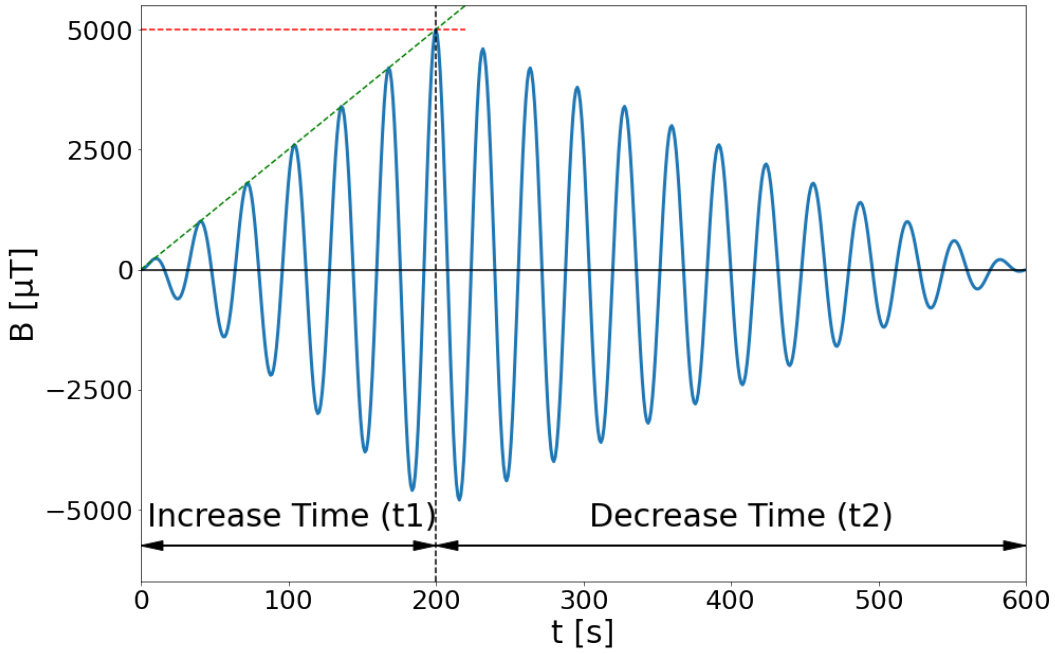

Figure 18: Magnetic field using for deperming.

On Fig. 18, we can see that the magnetic field is described by two slopes modulated by a sinusoidal function, one increasing and one decreasing. The magnetic field is being calculated using the code shown below:

```
import numpy as np
import math

#################
#DEPERM FUNCTION#
#################

def Deperm(f,Bmax,t1,t2,ts,Scale):
    #We define the total time the deperm is going to be active
    tt=t1+t2

    #We define the amount of steps it will take for the magnetic field to
    fully increase of decrease
    pasos1=math.floor(t1//ts)
    pasos2=math.floor(t2//ts)

    #We define the total amount of steps
    pasos=pasos1+pasos2

    #We define t like:
    t=np.zeros(pasos)
    for i in range(0,pasos):
        t[i]=i*ts

    #We define the slope of the hull (envolvente), in absolute value:
    m1=Bmax/t1
```

```
    m2=Bmax/t2

    #We find Bdeperm
    Bdeperm=np.zeros(pasos)
    for i in range(0,pasos1):
        Bdeperm[i]=m1*t[i]*math.sin(2*math.pi*f*t[i])
    ##################
    #This is a completly optinal process so that the slope doesn't suddenly
     change signs in the instant just after t1
    #This process only adds a global '-' to every Bdeperm after t1 if
    needed.
    #Variables:
    #d1 : Proportional value of the first derivative of B for t<t1 in the
    limit t->t1
    #d2 : Proportional value of the first derivative of B for t>t1 in the
    limit t->t1
    #dd1 : Proportional value of the second derivative of B for t<t1 in the
     limit t->t1
    #dd2 : Proportional value of the second derivative of B for t>t1 in the
     limit t->t1

    d1=math.sin(2*math.pi*f*t[pasos1])+2*math.pi*f*t[pasos1]*math.cos(2*
    math.pi*f*t[pasos1])
    d2=math.sin(2*math.pi*f*(t[i]))+2*math.pi*f*(t[i]-tt)*math.cos(2*math.
    pi*f*(t[i]))
    dd1=2*math.pi*t[i]*math.sin(2*math.pi*f*t[i])-2*math.cos(2*math.pi*f*t[
    pasos1])
    dd2=2*math.cos(2*math.pi*f*(t[i]))-2*math.pi*f*(t[i]-tt)*math.sin(2*
    math.pi*f*(t[i]))
    if d1<0:
        if d2<0:
            sgn=1
        elif d2>0:
            sgn=-1
        elif dd1<0:
            sgn=1
        else:
            sng=-1

    elif d1>0:
        if d2<0:
            sgn=-1
        elif d2>0:
            sgn=1
        elif dd2<0:
            sgn=-1
        else:
            sng=1
    elif dd1<0:
        if d2<0:
            sgn=1
        elif d2>0:
            sgn=-1
        elif dd2<0:
            sgn=1
        else:
            sng=-1
    else:
```

```
        if d2<0:
            sgn=-1
        elif d2>0:
            sgn=1
        elif dd2<0:
            sgn=-1
        else:
            sng=1
    ##################
    for i in range(pasos1,pasos):
        Bdeperm[i]=sgn*m2*(t[i]-tt)*math.sin(2*math.pi*f*(t[i]))

    #We find Vdeperm:
    Vdeperm=Scale*Bdeperm
    return t,Bdeperm,Vdeperm
```

Figure 19: Python code used for the deperm.

This code can be used to create any deperm function we desire, given the following inputs:

- f: Frequency of the oscilation (in Hz).
- $Bmax$: Maximum magnetic field applied (in μT).
- $t1$: time it takes for the magnetic field increases from 0 to Bmax (in s).
- $t2$: time it takes for the magnetic field decreases from Bmax to 0 (in s).
- ts: time our power generator holds each signal (in s).
- $Scale$: Relation between the magnetic field created an the power our current generator receives (in V/μT).

The code will then give us the following outputs:

- t : all moments of time where the current generator receives a signal (in s).
- $Bdeperm$: magnetic field for every moment of time (in μT).
- $Vdeperm$: voltage applied to the power generator for every moment of time (in V/μT).

In particular, Fig. 18 takes the inputs shown below:

f [Hz]	$Bmax$ [μT]	$t1$ [s]	$t2$ [s]	ts [s]	$Scale$ [V/μT]
1/32	5000	200	400	1	1/500

Table 2: Inputs used for Fig. 18 using the code given in Fig. 19.

4.2.3 Measuring in the MCF

For measuring, multiple magnetometers are placed inside the MCF. The magnetometers are placed in different locations, so that the measures of the magnetic field we get are as representative as possible. Each magnetometer will then measure the magnetic field an each direction.

One important thing to note is that most magnetometers have each direction sensors positioned in different places inside the magnetometer. In Yako's work [2] this wasn't consider, therefore leading in inaccurate results. The magnetometers we have used are Mag03-MS1000, and here below we can see an image of one [19]:

Figure 20: Image of the Mag03-MS1000 magnetometer used.

In Fig. 20 the X, Y and Z labels give an intuitive position of where the sensors for each directions are, but since we need to be as precise as possible we will use the positions given in the outline drawings [20] for a Mag03-MS:

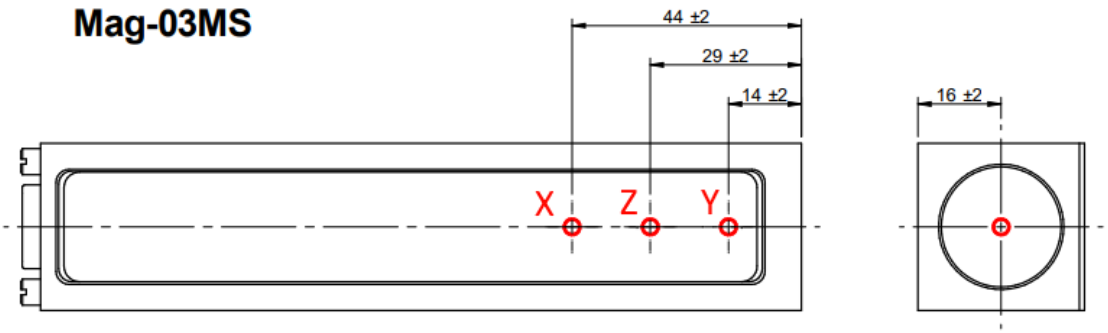

Figure 21: Position of each sensor in a Mag03-MS magnetometer (distances given in mm).

Since this is a recurring problem for our measurements and it must be taken into a

count, we must find a way to store this information efficiently. From Fig. 20 and Fig. 21 we can see that this offsets only appear in the Z axis of the magnetometer a efficient way of displaying this information will be as follows:

OFFSET	Mag. [cm]
Sensor X	-1.5$\hat{z}$
Sensor Y	1.5$\hat{z}$
Sensor Z	0

Table 3: Offset for a the magnetometer seen in Fig. 20 and Fig. 21.

Note that we have added a $\hat{z}$ to express that this offset is on the Z axis. This won't always be the case since, as we will see late, the magnetometers axis from Fig. 20 do not always coincide with the X, Y and Z axis we have set for out reference frame.

Before we move on we also have to mention that there is a small discrepancy between the distances found in Fig. 21 and the ones we were given by ESA. In Fig. 21 the distance between the Y and Z sensors is 15 ± 2 mm, meanwhile the distance we were given is 16 ± 1 mm. This may be due to using the documentation for a Mag03-MS magnetometer instead of a Mag03-MS1000, but since no outline drawings nor documentation for Mag03-MS1000 could be found, this is the best way to illustrate where the sensors are located; even is the distances are not completely on point.

It is important to note that the direction of the axes X, Y and Z does not coincides with those of Fig. 17, since the magnetometer can take different orientations depending of how it is placed inside the MCF. Here below we can see images of how three different magnetometers are placed inside the MCF:

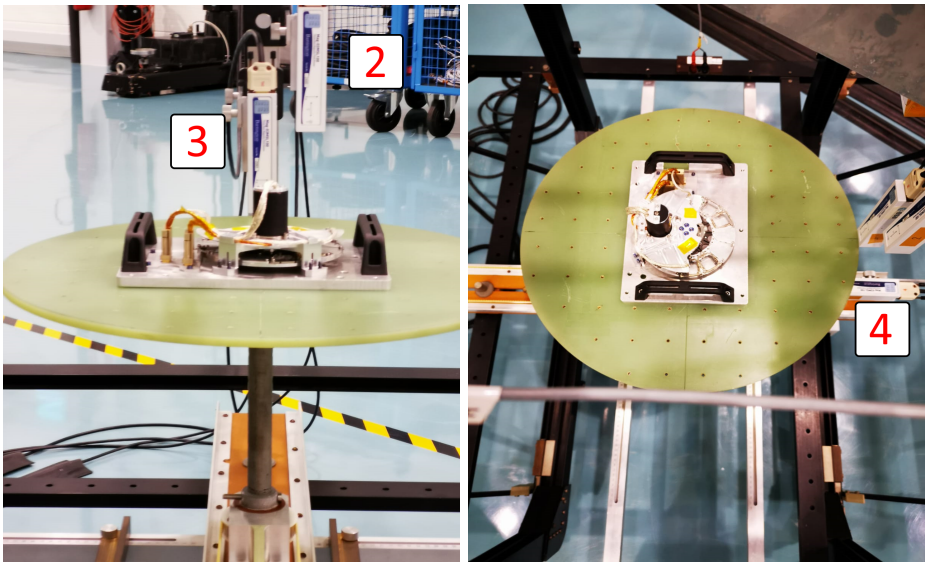

Figure 22: Position of each magnetometers 2, 3 and 4.

In the case of Fig. 22 the numbers 2, 3 and 4 each represent a magnetometer. Magnetometers 2 and 3 have the same orientation but magnetometer 4 is set horizontally. In neither of these magnetometer the axes from Fig. 20 coincide with those of Fig. 17. In this particular case, the readings from the magnetometers $B_{i\ Mag}$ should be interpreted

as follows:

	Mag. 2	Mag. 3	Mag. 4
B_x	$B_{y\ Mag}$	$B_{y\ Mag}$	$-B_{z\ Mag}$
B_y	$B_{x\ Mag}$	$B_{x\ Mag}$	$B_{x\ Mag}$
B_z	$-B_{z\ Mag}$	$-B_{z\ Mag}$	$-B_{y\ Mag}$

Table 4: Example of interpretations of the readings given by the magnetic field.

Now that everything is set, we are ready to measure. The object we want to study is placed in the middle plate, which can be seen on the pictures from Fig. 15 and the Fig. 16. This circular plate is set on the middle of the facility and allows the object to be spun. This spinning movement allows us to measure the magnetic field all around the object, without having to move our magnetometers. Using the magnetometers from Fig. 22, the points where the magnetic field will be measured is shown in the figures below:

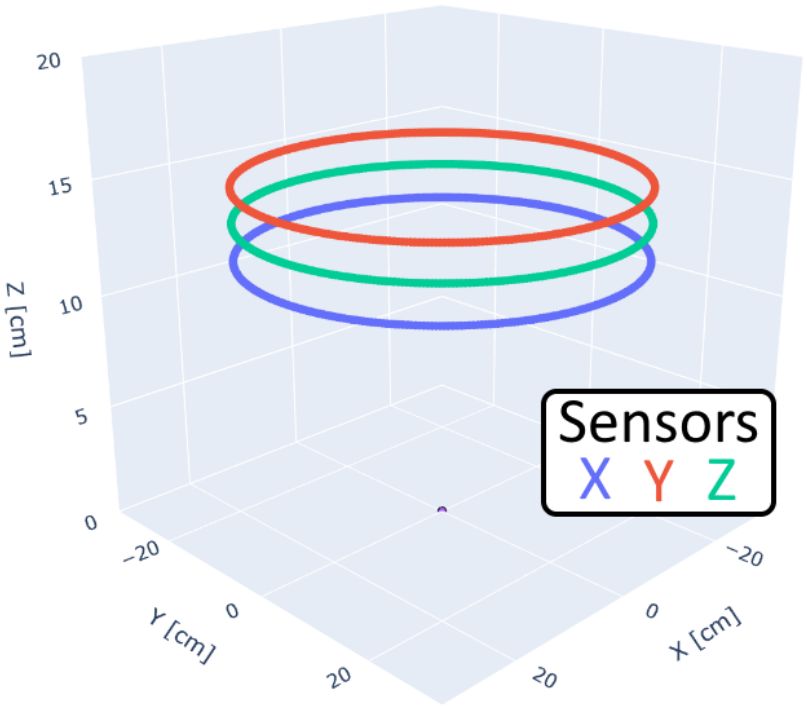

Figure 23: Position of Magnetometer 2 from Fig. 22 during the measurement process.

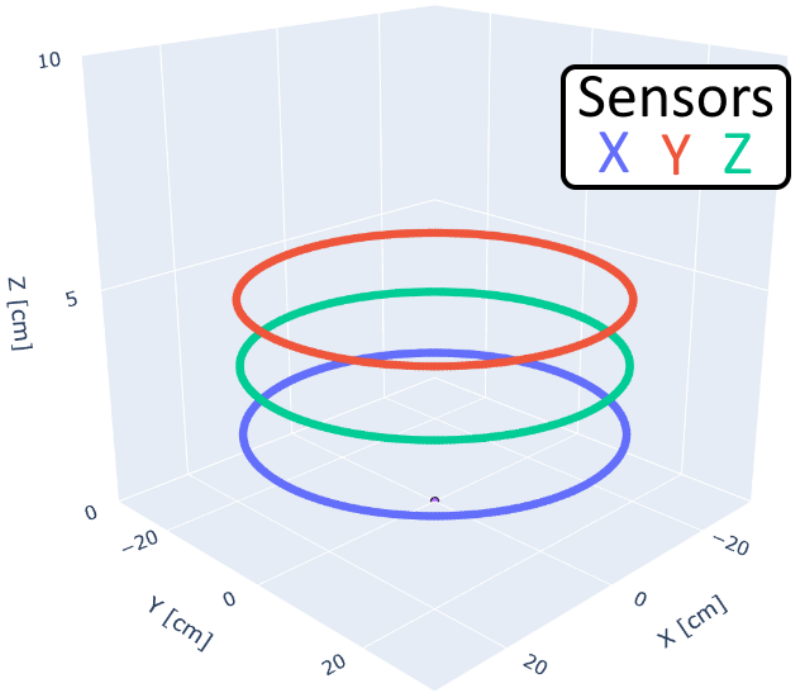

Figure 24: Position of Magnetometer 3 from Fig. 22 during the measurement process.

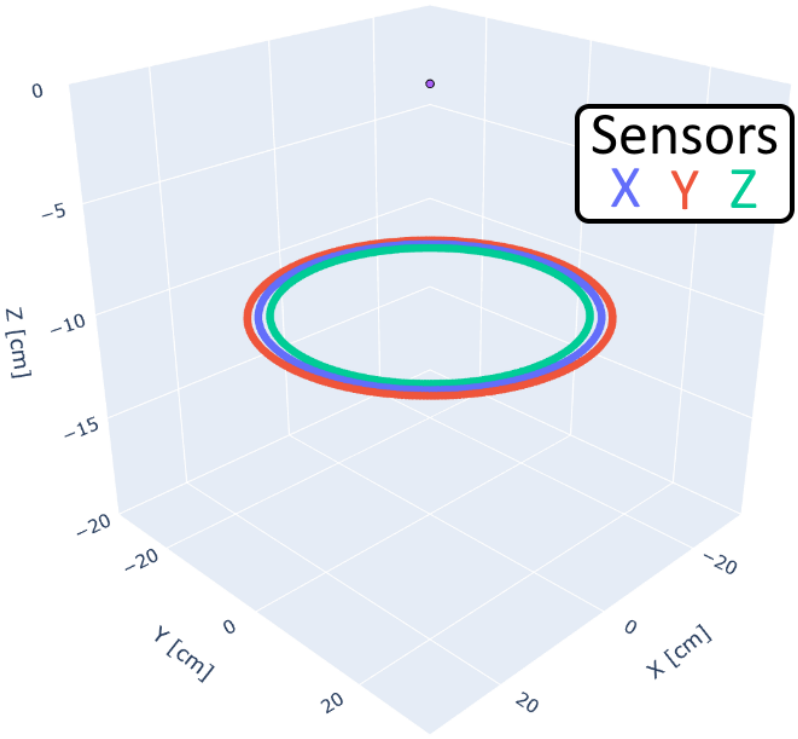

Figure 25: Position of Magnetometer 4 from Fig. 22 during the measurement process.

In figures above the blue, red and green points represent the positions where the B_x, B_y and B_z components of the magnetic field are being measured, respectively; and the

purple dot found in all of the plots represents the origin.

4.3 Optimization algorithm

This section is dedicated to explain the intricacies of the optimization algorithm used. In our case, this algorithm will be a Particle Swarm Optimization method or PSO. The PSO algorithm is an heuristic algorithm. The name of this algorithm comes from its inspiration from bird, where each individual moves not only based on its position, but also on the position of the rest of the individuals that form the swarm. The swarm then, tries to find a position where a desired function is better optimized [21].

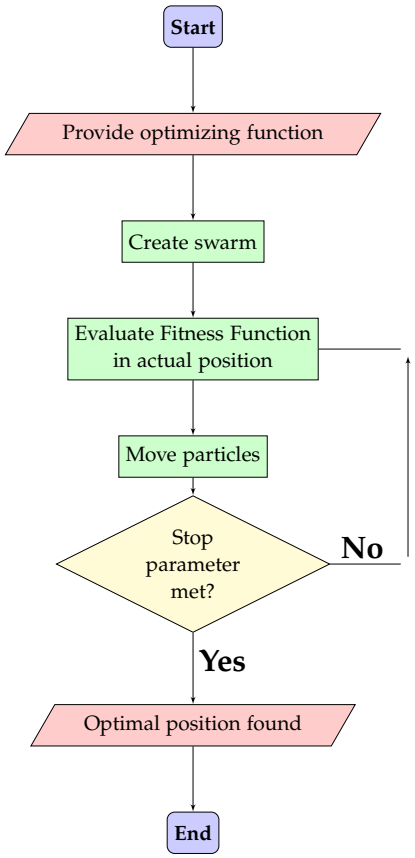

Figure 26: Flow chart of the PSO algorithm.

4.3.1 PSO Algorithm

The foundation of this algorithm is based on four steps [21]:

1. Create an initial swarm, with a set number of particles, at a random starting point inside of the given limits. Each particles possess four elements: its position, the value of the optimizing function, a register of the best position so far and its current velocity.
2. Evaluating each particle with the optimizing function F.
3. Updating the position and velocity of each particle. This is what gives the algorithm the optimization property.
4. If the stop parameters are not met, return to step 2.

The velocity and position of the particles is updated via the following expressions [21]:

$$v_i(t+1) = wv_i(t) + c_1 r_1[\mathcal{X}_i(t) - x_i(t)] + c_2 r_2[g(t) - x_i(t)] \tag{4.6}$$

$$x_i(t+1) = x_i(t) + v_i(t+1)\ , \tag{4.7}$$

where we identify the following variables:

- $v_i(t)$: velocity of the particle i in the instant t.
- w: inertia coefficient.

- c_1: cognitive coefficient.
- c_2: social coefficient.
- $\mathcal{X}_i(t)$: best position the particle i has been so far.
- $x_i(t)$: current position of the particle i.
- $g(t)$: best position found by the swarm globally.
- r_1 and r_2: random numbers between 0 and 1.

In particular, for our calculations we have used the following parameters:

w	c_1	c_2
1	1.5	1.5

Table 5: Parameters used in our PSO programs.

Since this is an iterative process we also have to define stop parameters. In our case, this parameters consist of a maximum of 700 iterations and a stop tolerance of $10 \cdot 10^{-7}$, which refers to the minimal value the fitness function F has to vary between iterations for the optimization to continue.

4.3.2 Fitness function

Now that we have defined our algorithm, we have to define a fitness function F. This section will follow the work of Elisa Carrubba, Axel Junge, Filippo Marliani, and Agostino Monorchio. *Particle swarm optimization to solve multiple dipole modelling problems in space applications* [22].

First, we will start by using the least square function F_1, defined as follows:

$$S = \left(\sum_{i=0}^{360} \left[\left(B_x^{(meas)}[i] - B_x^{(PSO)}[i] \right)^2 + \left(B_y^{(meas)}[i] - B_y^{(PSO)}[i] \right)^2 + \left(B_z^{(meas)}[i] - B_z^{(PSO)}[i] \right)^2 \right] \right)^{1/2} \tag{4.8}$$

$$F_1 = \frac{S}{\sqrt{\sum_{i=0}^{360} \left[\left(B_x^{(meas)}[i] \right)^2 + \left(B_y^{(meas)}[i] \right)^2 + \left(B_z^{(meas)}[i] \right)^2 \right]}}, \tag{4.9}$$

where i refers to the angle in degrees. Notice that, in case we would want to take F_1 as our fitness function, S would do the work just fine, since the denominator of F_1 is a constant. This denominator is necessary for F_1 to be included in F. Also note that, since F_1 represents the mean square function, it will also be a good indicator of the goodness of our fit.

We also define the least mean function F_2:

$$F_2 = \frac{\sum_{i=0}^{360}\left(B_x^{(meas)}[i] - B_x^{(PSO)}[i]\right)^2}{\sum_{i=0}^{360}\left(B_x^{(meas)}[i]\right)^2} + \frac{\sum_{i=0}^{360}\left(B_y^{(meas)}[i] - B_y^{(PSO)}[i]\right)^2}{\sum_{i=0}^{360}\left(B_y^{(meas)}[i]\right)^2} + \\ + \frac{\sum_{i=0}^{360}\left(B_z^{(meas)}[i] - B_z^{(PSO)}[i]\right)^2}{\sum_{i=0}^{360}\left(B_z^{(meas)}[i]\right)^2} \quad . \tag{4.10}$$

Finally, we define the fitness function F as a combination of (4.9) and (4.10) [22]:

$$F^{(n)} = F_2^{(n)}\left(\frac{F_2^{(n-1)}}{F_1^{(n-1)}}\right) + F_1^{(n)}\left(\frac{F_1^{(n-1)}}{F_2^{(n-1)}}\right) \ , \tag{4.11}$$

where n refers to the current iteration and $n-1$ to the previous one. For iteration $n = 0$ the values of $F_1^{(n-1)}$ and $F_2^{(n-1)}$ are set randomly.

The PSO code that will be used for our tests can be found in GranaSAT's github repository [5] under the name *PSO_VICTOR*. This code allows us to select three different modeling methods, along with their approximated running time, if the magnetic field is measured by 3 magnetometers:

Method	1 Dipole	2 Dipoles	1 Dipole and 1 Quadrupole
t_{ex} [s]	130	140	240

Table 6: Running times of the PSO algorithm for each method.

The magnetic field for the dipoles will be given by expressions (2.16), meanwhile for the quadrupole we will use expressions (2.26) to find the magnetic field of 2 current loops separated by the same distance as their diameter with currents flowing in opposite directions.

This program can also be set to compare the three methods if desired, and adding more magnetometers adds ≈ 30 s to each running time. It must be noted that this running times have been done in a 11th Gen Intel(R) Core(TM) i7-11800H 2.30GHz processor and 16.GB of RAM [23].

5 Results and discussion

5.1 The importance of deperming

First we will check the importance of the deperming process. For that, we will compare the magnetic field of a filter wheel before and after deperming. For this process, our magnetometers are set in the positions given in Tab. 7 along with the offsets Tab. 8.

Position	Mag. 2	Mag. 3	Mag. 4
x [±1 cm]	36.7	36.7	32.4
y [±1 cm]	-5.4	0.0	-5.4
z [±1 cm]	13.5	3.5	-9.7

Table 7: Position of the magnetometers for checking the importance of the deperming process (FAR Config.).

OFFSET	Mag. 2 [cm]	Mag. 3 [cm]	Mag. 4 [cm]
Sensor X	-1.6$\hat{z}$	-1.6$\hat{z}$	0
Sensor Y	1.5$\hat{z}$	1.5$\hat{z}$	1.5$\hat{x}$
Sensor Z	0	0	-1.6$\hat{x}$

Table 8: Offsets for the magnetometers from Tab. 7.

Now we will compare the X component on the magnetic field for the three magnetometers, before and after the deperming process:

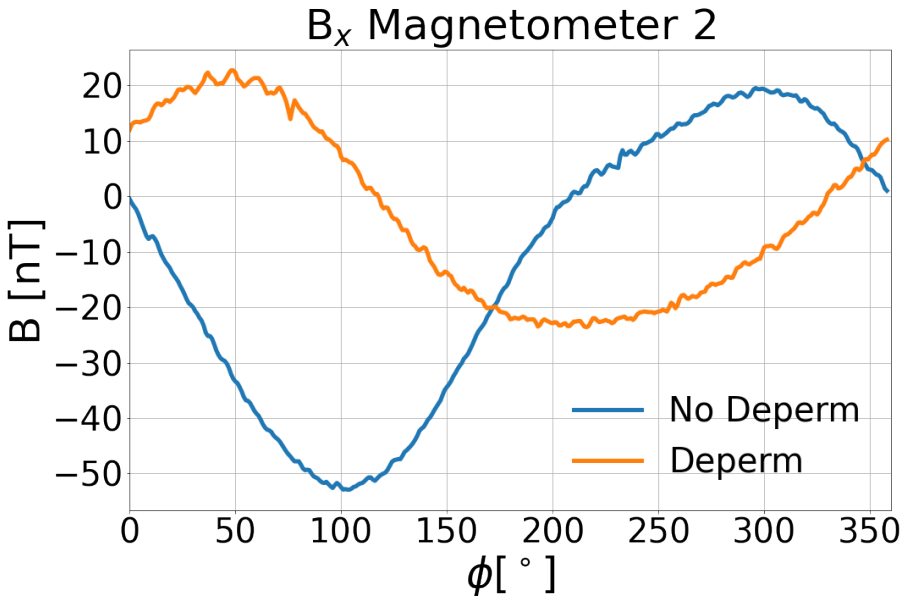

Figure 27: X component on the magnetic field for a filter wheel before and after deperming for Magnetometer 2, whose position can be found in Tab. 7.

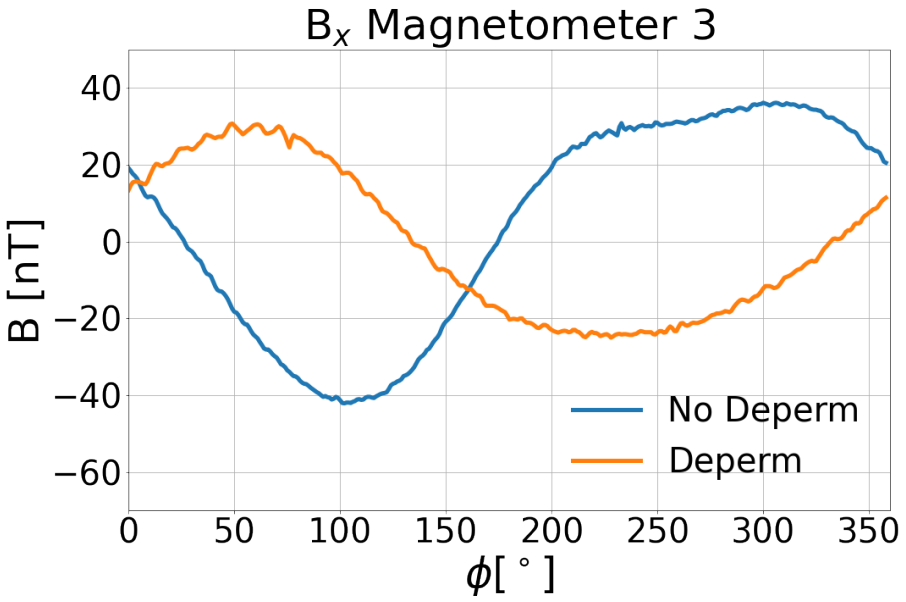

Figure 28: X component on the magnetic field for a filter wheel before and after deperming for Magnetometer 3, whose position can be found in Tab. 7.

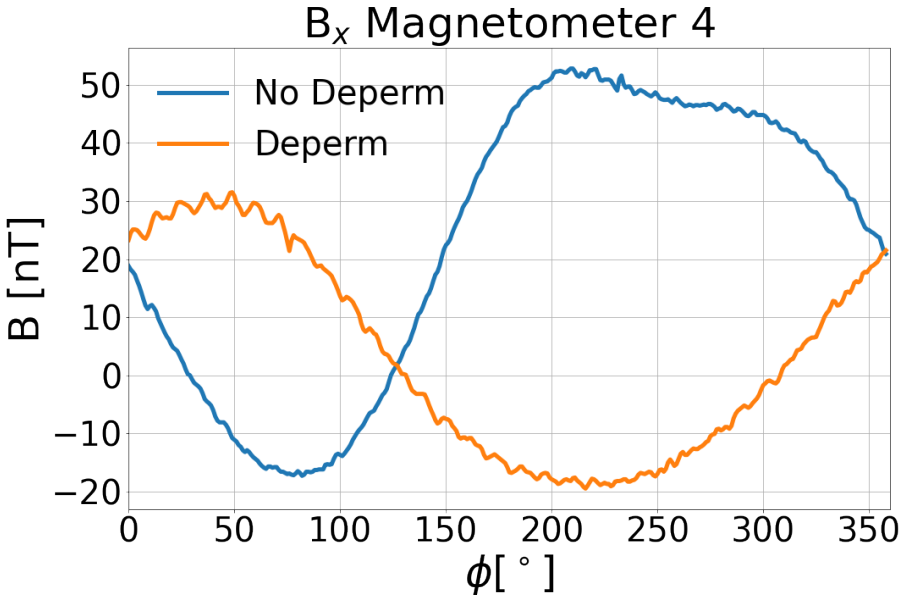

Figure 29: X component on the magnetic field for a filter wheel before and after deperming for Magnetometer 2, whose position can be found in Tab. 7.

As we can see, the magnetic fields are completely different, so if we want to get a faithful measure for the magnetic field of an electronic component we must apply a deperming process first. However, the rest of the data we were given by ESA has not been depermed before, for what we can assume are simplicity reasons, since this process can take a moderate amount of time to perform.

5.2 Comparing Our PSO Data with ESA's

In this section we will study the magnetic field created my a motor. For this measures, four magnetometers have been placed inside the MCF, in the following positions:

Position	Mag. 1	Mag. 2	Mag. 3	Mag. 4
x [±1 cm]	22.4	26.7	26.7	22.4
y [±1 cm]	0.0	-5.4	0.0	-5.4
z [±1 cm]	32.3	13.5	3.5	-9.7

Table 9: Position of the magnetometers for measuring the magnetic field of a motor.

OFFSET	Mag. 1 [±2 cm]	Mag. 2 [±2 cm]	Mag. 3 [±2 cm]	Mag. 4 [±2 cm]
Sensor X	0	-1.6$\hat{z}$	-1.6$\hat{z}$	0
Sensor Y	1.5$\hat{x}$	1.5$\hat{z}$	1.5$\hat{z}$	1.5$\hat{x}$
Sensor Z	-1.6$\hat{x}$	0	0	-1.6$\hat{x}$

Table 10: Offsets for the magnetometers from Tab. 9.

For this algorithm, the PSO given by ESA is given by just 1 dipole, so that is what we will try to replicate with our PSO algorithm. Here below lies a comparison between the results given by both optimization algorithms:

	Coordinates [cm]			Magnetic moment [mAm^2]			
	x_0	y_0	z_0	m_x	m_y	m_z	F_1
ESA	-0.2	0.4	1.7	1.123	-65.17	-0.288	2.9%
GranaSAT	-0.2	0.31	1.8	0.608	-65.73	0.599	3.4%

Table 11: Comparison of the PSO results for a 1 dipole model for a motor.

As we can see in Tab. 11, the approximation given by ESA is better than the one we get. This could be remedied by running the PSO program multiple times until we find a better result. Here below we can see how both approximations hold against the measured data:

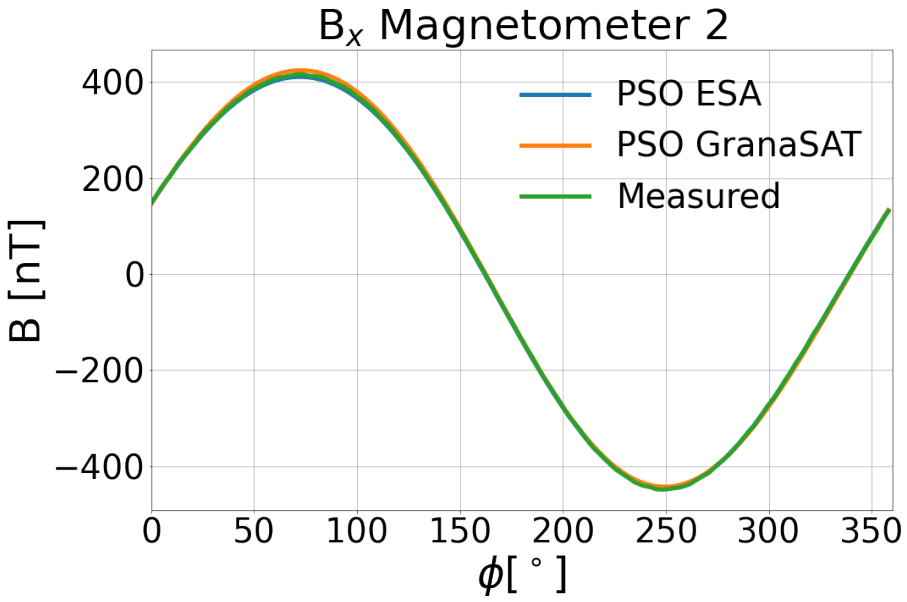

Figure 30: X component on the magnetic field for a motor for Magnetometer 2, whose position can be found in Tab. 9.

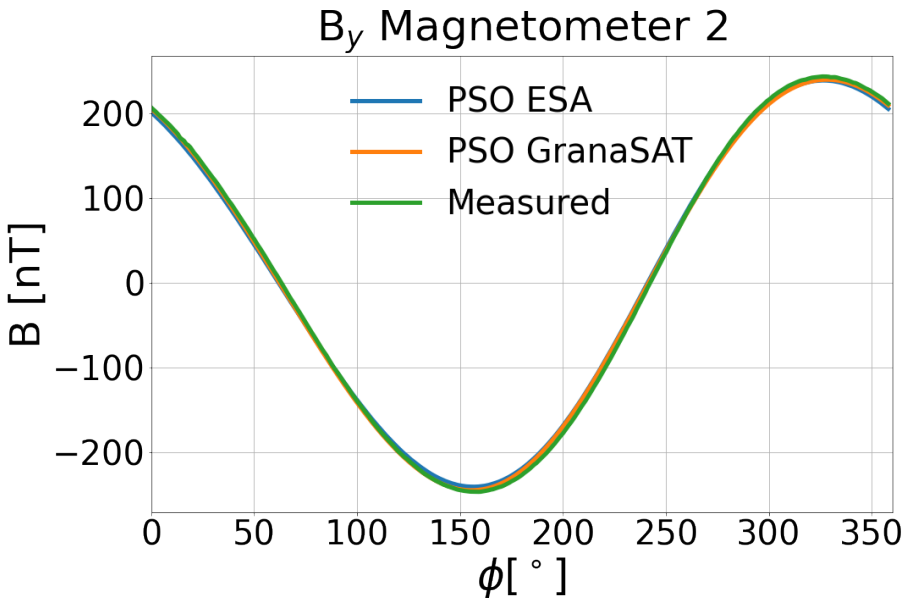

Figure 31: Y component on the magnetic field for a motor for Magnetometer 2, whose position can be found in Tab. 9.

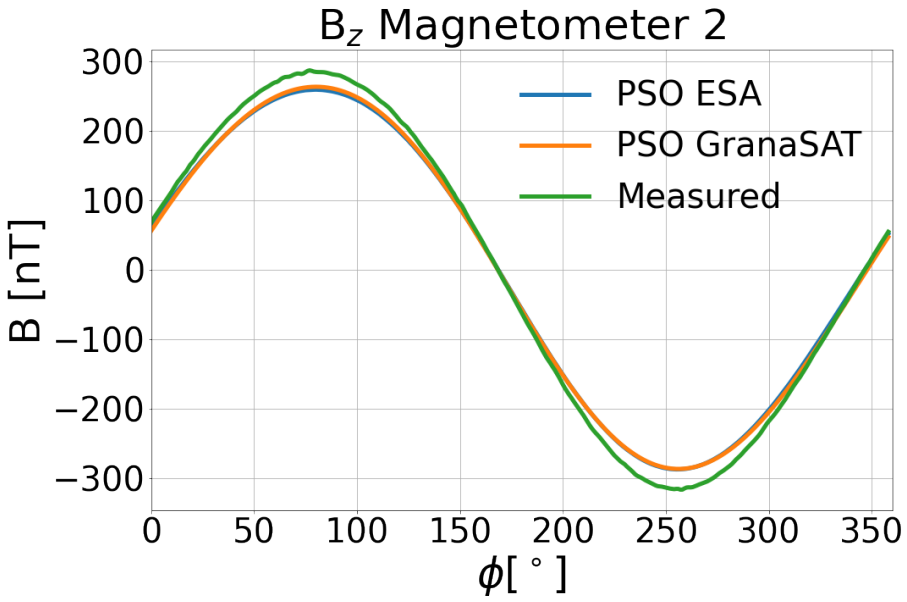

Figure 32: Z component on the magnetic field for a motor for Magnetometer 2, whose position can be found in Tab. 9.

We have decided to only show the graphs for magnetometer 2 to avoid redundancy, since the results we get for the rest of magnetometers are very similar. As we can see, both approximations hold pretty well against the measured data. We can also check for the relative errors:

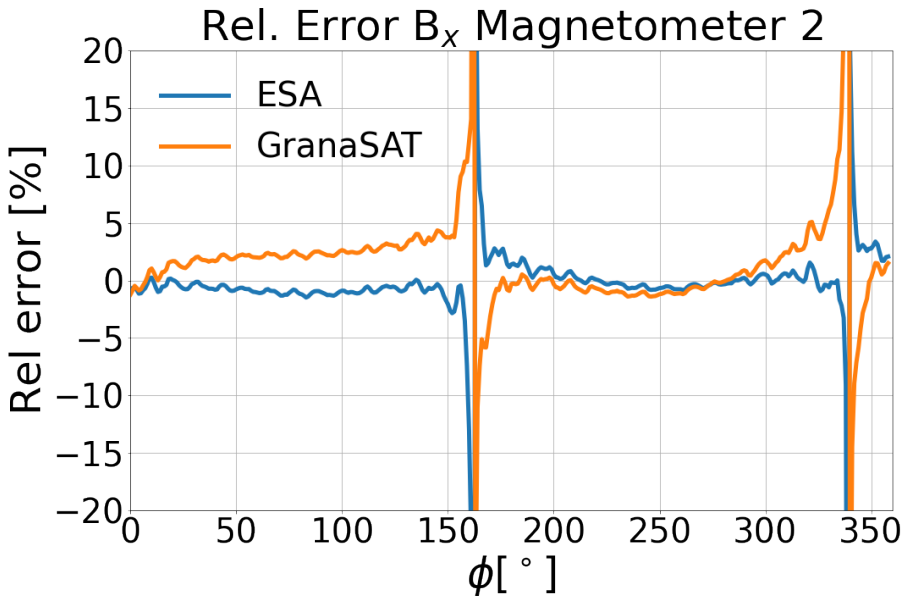

Figure 33: Relative error of the X component on the magnetic field for a motor for Magnetometer 2 from Fig. 30.

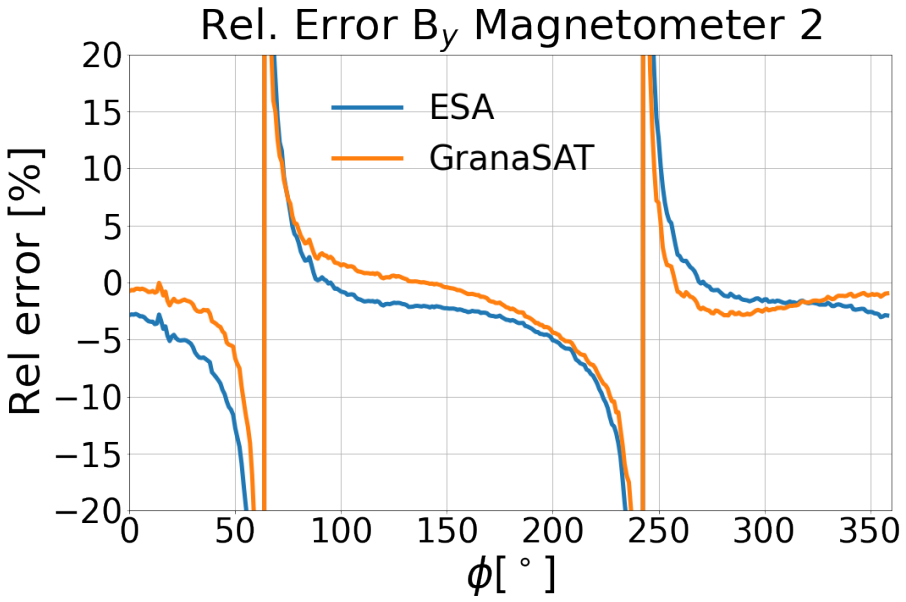

Figure 34: Relative error of the Y component on the magnetic field for a motor for Magnetometer 2 from Fig. 31.

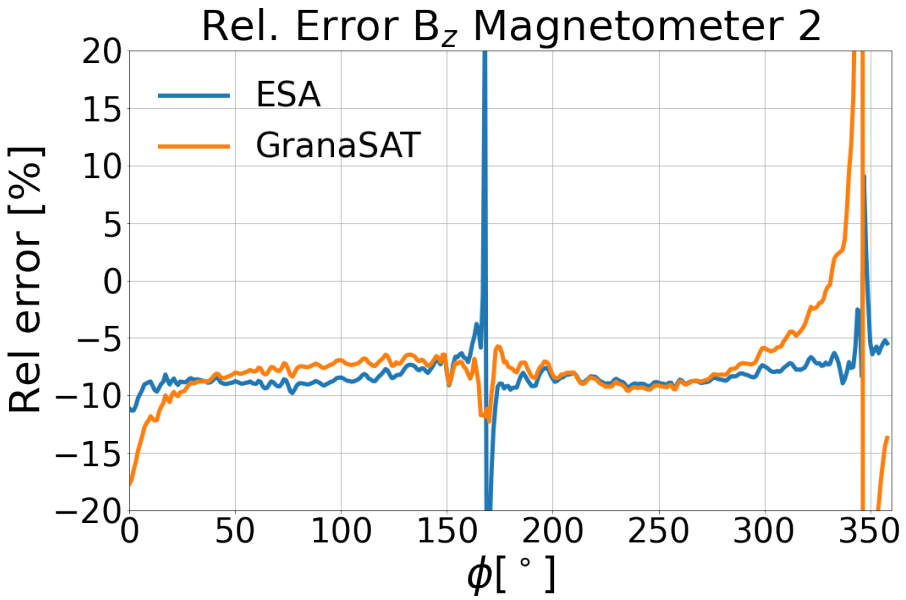

Figure 35: Relative error of the Z component on the magnetic field for a motor for Magnetometer 2 from Fig. 32.

In Fig. 33, 34 and 35 we can see that the errors skyrocket for the values where the magnetic field measured is 0, but stays below 5% for the most part otherwise.

5.3 Validity of approximations

Now we will compare how the distance we measure can affect the results we get in our optimization problem. We will consider two different scenarios for the filter wheel

magnetic field. The first one is given by Tab. 7 and Tab. 8 and the second one given by the following:

Position	Mag. 2	Mag. 3	Mag. 4
x [±1 cm]	26.7	26.7	22.4
y [±1 cm]	-5.4	0.0	-5.4
z [±1 cm]	13.5	3.5	-9.7

Table 12: Position of the magnetometers for measuring the magnetic field of a filter wheel (NEAR Config.).

The second scenario has the same offsets given by Tab. 8. We also can see that the differences between Tab. 7 and Tab. 12 lies solely in that the magnetometers have been brought 10 cm closer in the X axis. Because to this, we will name the first configuration FAR and the second NEAR.

For each scenario 10 simulations have been run for each model, leading to a total of 60 simulations. The best approximations for each can be found below:

	Coordinates [cm]			Magnetic moment [mAm^2]		
	x_0	y_0	z_0	m_x	m_y	m_z
Dipole	-4.7	-0.5	2.9	2.43	9.11	-9.78

	Coordinates [cm]			Orientation [°]		Current Loop [°]		
	x_0	y_0	z_0	θ	φ	a [cm]	I [A]	F_1
Quadrupole	2.00	-1.39	0.39	90	291	9.6	-1.39	6.1%

Table 13: Best approximation for the magnetic field of a filter wheel for the FAR scenario.

	Coordinates [cm]			Magnetic moment [mAm^2]			
Dipole	x_0	y_0	z_0	m_x	m_y	m_z	F_1
1	-3.0	-0.6	7.7	4.70	1.32	-6.09	10.7%
2	2.3	2.8	1.4	0.66	-6.25	-3.17	

Table 14: Best approximation for the magnetic field of a filter wheel for the NEAR scenario.

In the case of NEAR, the best approximation is given by the 2 dipole model, meanwhile for FAR the best model is 1 dipole and 1 quadrupole. This is surprising, since in theory the quadrupole approximation becomes worse at further distances, yet in our case it is better to use 1 dipole and 1 quadrupole for the scenario where the magnetometers are further away. The only reason we can give for this is that, at the end of the day, these are just approximations of a magnetic field that has an intricate shape, and specially since the distance between the distance of both scenarios is not that big, our intuition may be misleading.

One thing that may be interesting to test is how well does the FAR approximation hold in the the positions where the scenario NEAR is measured, and vice versa. Here below we can see this comparison:

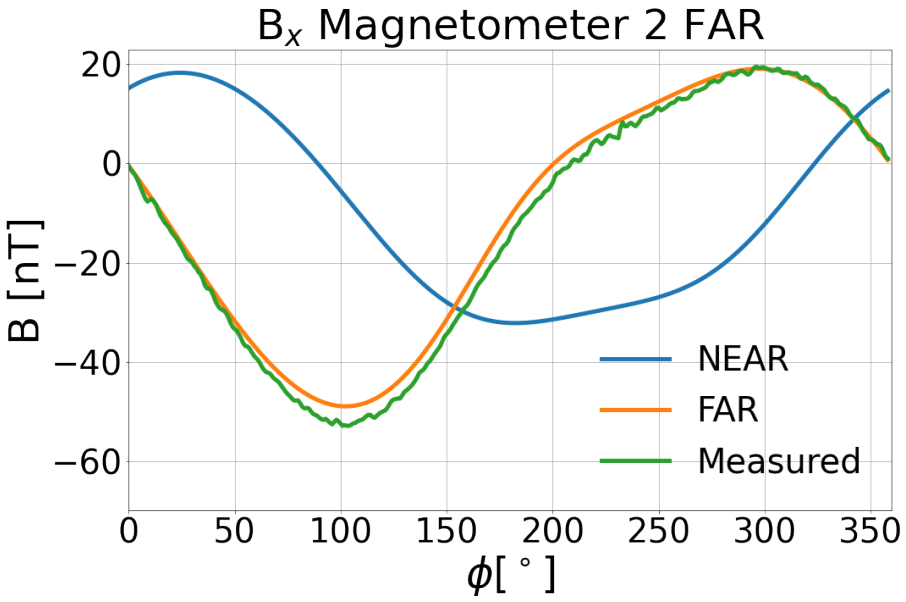

Figure 36: Comparison between the X component of the magnetic field created by a filter wheel using the approximations FAR and NEAR, in the positions points where FAR is measured.

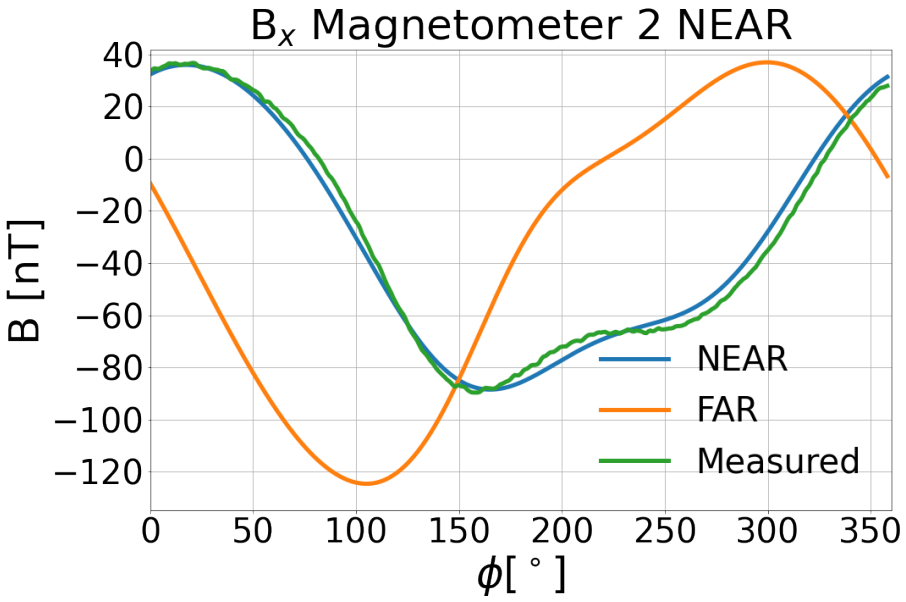

Figure 37: Comparison between the X component of the magnetic field created by a filter wheel using the approximations FAR and NEAR, in the positions points where NEAR is measured.

As we can see, the approximations do not hold outside of the positions they have been calculated. We can conclude that, if we wish to approximate any electronic product using dipoles and quadrupoles, not only does the device have to be depermed before; but in general the approximation will only hold in the points the magnetic field was measured to do such approximation, or close to them.

6 Conclusions

To conclude, we will summarize the different activities accomplished during this thesis:

- First, we expanded previous works by adding the quadrupole approximation to our algorithms. Not only that, but we also found an alternative way to treat magnetic quadrupole by the use of current loops described by elliptic integrals, which has proven to be a very efficient way of computing magnetic quadrupoles, as seen in Tab. 1.
- We have created a program for soft iron calibration, this is, the calibration of the magnetometer. We have also created a program for the demagnetization process of an object, also known as deperm.
- We also improved Yako's work [2], by considering that each sensor in a magnetometer is in a different position as the datasheets from these products suggest [20].
- Finally, we have used some experimental data provided by ESA of different electronic components and studied them. We concluded that the deperm process is very important if we desire to get a good measure of the magnetic field of an electronic device, as seen on Fig. 27, Fig. 28 and Fig. 29. We also compared our PSO program with those of ESA, leading to similar results; and concluded that dipole and quadrupole approximations in general only hold in the points where the magnetic field is measured to do such approximations or in their vicinity, as we can see on figures Fig. 36 and Fig. 37.
- The most remarkable part of our work is that most of the things we have accomplished come in terms of Python code, which expands to a total of 5657 lines of code, which can be accessed by anyone at GranaSAT's GitHub repository [5].

Now, as a final note, we will discuss what parts of our work could be improved:

- In Fig. 19, the function takes the input $Vdeperm$, yet we have not made use of this. It is left to future works to make use of this to apply a deperm process in our own MCF.
- The code is one of the main component of this thesis and, since I had not worked with Python before, I am sure it could be optimised to run faster. Not only that, but it could also be made 'prettier' by adding an actual interface to the programs. The PSO program could also be improved by allowing it to work with as many dipoles and quadrupoles as desired. It could also be made so multiple optimizations can be run on multiple cores of the CPU at the same time, but that is outside of the scope of this thesis.
- Since our objects of study are electronic devices, the magnetic field should be measured having our object in ON and OFF states. For simplicity all the measurement have been done in an OFF state, but it is possible that the magnetic field varies if set to ON.

References

[1] *Ulysses*. NASA. URL: https://solarsystem.nasa.gov/missions/ulysses/in-depth/.

[2] Yako Irusta Salles. "Optimizer to obtain the magnetic equivalent of a small satellite". Bachelor's Thesis. Universidad de Granada, June 2021. URL: https://digibug.ugr.es/handle/10481/74457.

[3] Pedro Manuel Vizcaíno Delgado. "*Platform for the measuremet of an electronic product's magnetic moment.*" PhD thesis. Universidad de Granada, June 2020. URL: https://digibug.ugr.es/handle/10481/74465.

[4] European Space Agency. URL: https://www.esa.int/.

[5] *PSO-Algorithm-to-solve-Multipolar-Modeling-problems*. GranaSAT. URL: https://github.com/granasat/PSO-Algorithm-to-solve-Multipolar-Modeling-problems.

[6] *JupyterLab Documentation*. URL: https://jupyterlab.readthedocs.io/en/stable/index.html.

[7] David J. Griffiths. *Introduction to electrodynamics*. Cambridge University Press, 2018. ISBN: 9781107189638.

[8] Carl Rod Nave. *HyperPhysics, Quadrupole Magnetic Field*. 2000. URL: http://hyperphysics.phy-astr.gsu.edu/hbase/magnetic/magquad.html#:~:text=Two%20properly%20spaced%20coils%20with,produce%20a%20magnetic%20quadrupole%20field..

[9] John David Jackson. *Classical electrodynamics*. 3rd ed. New York, NY: Wiley, 1999. ISBN: 9780471309321.

[10] Carl Rod Nave. *HyperPhysics, Magnetic Field of Current Loop*. 2000. URL: http://hyperphysics.phy-astr.gsu.edu/hbase/magnetic/curloo.html.

[11] James Simpson et al. "Simple Analytic Expressions for the Magnetic Field of a Circular Current Loop.". NASA, Jan. 2001.

[12] A. Ghaith et al. "Permanent Magnet-Based Quadrupoles for Plasma Acceleration Sources". In: *Instruments* 3 (Apr. 2019), p. 27. DOI: 10.3390/instruments3020027.

[13] Merlin Oz. *Sailboat Instruments*. Accesed via Internet Archive: 2022-05-06. URL: http://web.archive.org/web/20201019170034/https://sites.google.com/site/sailboatinstruments1/home.

[14] *LSM9DS0. iNEMO inertial module: 3D accelerometer, 3D gyroscope, 3D magnetometer*. STMicroelectronics. Mar. 2015. URL: https://cdn-shop.adafruit.com/datasheets/LSM9DS0.pdf.

[15] *Arduino Pro Mini*. URL: https://docs.arduino.cc/retired/boards/arduino-pro-mini.

[16] *Magnetic Field Calculators*. National Centers For Enviromental Information.

[17] *MAGNETIC COIL FACILITY AT ESTEC*. European Space Agency, Sept. 2019. URL: https://sci.esa.int/web/lisa-pathfinder/-/45846-magnetic-coil-facility.

[18] *Electromagnetic compatibility*. Tech. rep. ECSS-E-ST-20-07C Rev. 1. Feb. 2012. URL: http://everyspec.com/ESA/download.php?spec=ECSS-E-ST-20-07C_REV-1_07FEB2012.047904.pdf.

[19] *Operation manual for Mag-03 Three-Axis Magnetic Field Sensors*. OM1004/28. Bartington Instruments Limited. URL: https://manualzz.com/doc/23439031/mag-03-three-axis-magnetic-field-sensor.

[20] Daniel Cetnik. *Mag-03MS Outline Drawing*. Bartington Instruments. URL: https://gmw.com/wp-content/uploads/2021/04/Mag-03MS_DR2587.pdf.

[21] Joaquín Amat Rodrigo. *"OPTIMIZACIÓN PSO CON PYTHON"*. URL: https://joaquinamatrodrigo.github.io/optimizacion_PSO_python/.

[22] Elisa Carrubba et al. "Particle swarm optimization to solve multiple dipole modelling problems in space applications". In: *2012 ESA Workshop on Aerospace EMC*. IEEE. May 2012. URL: https://www.semanticscholar.org/paper/Particle-Swarm-Optimization-to-solve-Multiple-in-Carrubba-Junge/5e5c6d2e0bf1d2c9b831af8b1b046aeb2a3bfc6b#citing-papers.

[23] *OMEN 16 Laptop*. URL: https://www.omen.com/es/es/laptops/2021-omen-16-intel/specifications.html.

Propuesta de Trabajo Fin de Grado en Física

Tutor/a:	**Prof. Andrés Roldán Aranda**
Departamento y Área de Conocimiento:	**Electrónica y Tecnología de los computadores**
Email:	**amroldan@ugr.es**

Título del Trabajo: **Medida del momento magnético de un producto electrónico usando fluxgates 3D**

Tipología del Trabajo: *(Segun punto 3 de las Directrices del TFG aprobadas por Comisión Docente el 10/12/14)*

(Marcar con X)

1. Revisión bibliográfica		*4. Elaboración de nuevas prácticas de laboratorio*	
2. Estudio de casos teórico-prácticos		*5. Elaboración de un proyecto*	
3. Trabajos experimentales	*X*	*6. Trabajo relacionado con prácticas externas*	

Breve descripción del trabajo:

La medida de las características magnéticas de los productos electrónicos es muy necesaria para conocer el comportamiento del producto y obtener su modelo simplificado. Esta técnica es más importante cuando se trata de una parte de un satélite [1] que debe soportar el boom donde se realiza la medida del campo magnético exterior cercano a un planeta. Los subsistemas del satélite deben estar caracterizados para que a partir de la medida 3D del campo exterior y descontando lo aportado por el satélite, se pueda medir con precisión el campo magnético existente en un punto del espacio.

Para ello se simplifica el comportamiento de un producto mediante un conjunto de dipolos magnéticos residuales que se caracterizan mediante medidas sistemáticas en el laboratorio, figura 1. Se usará la técnica de caracterización basad en dos magnetómetros 3D del tipo fluxgate y MEMS existentes en el laboratorio.

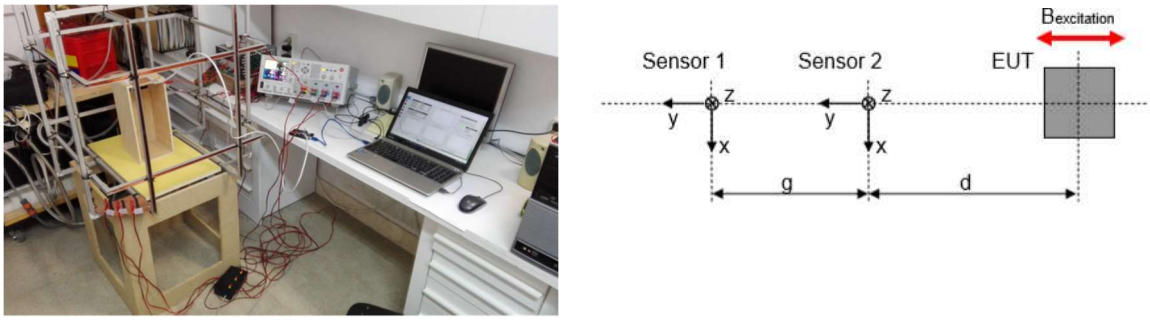

Figura 1. Sistema de medida del momento magnético. Configuración con dos magnetómetros 3D.

Objetivos planteados:

Se realizará el setup de medida para la caracterización de la inducción generada por un campo externo producido por unos carretes de Helmholtz y una fuente de corriente controlada mediante Python.

Se testearán varios equipos electrónicos e imanes permanentes de neodimio y se les obtendrá el modelo

magnético dipolar..

Es estudiante trabajará en el Laboratorio del Grupo de Electrónica Aeroespacial de la UGR. Se busca estudiante interesado en aplicaciones experimentales.

Metodología:

El alumno comenzará el trabajo leyendo la documentación que el tutor tiene preparada donde se describen las técnicas de modelado, simulación y medida. Para el análisis vectorial [2] previo se usarán los notebook de Jupyter en Python. Las simulaciones y medidas de los magnetómetros 3D (fluxgates) se realizarán con Arduino y el control de las bobinas con Python o similar

Bibliografía:

[1] ECSS-E-ST-20-07C-Rev1 - 7 February 2012.
[2] Magnetic Moment easy measurement.

Pinchar aquí para ver otros trabajos anteriores realizados por alumnos del Grado en Física.

A rellenar sólo en el caso que el alumno sea quien realice la propuesta de TFG
Alumno/a propuesto/a: SIN ASIGNAR

Granada, 20 de mayo 2020
Sello del Departamento